Synthesis, Structural, Magnetic, and Redox Properties of Asymmetric Diiron Complexes with a Single Terminally Bound Phenolate Ligand. Relevance to the Purple Acid Phosphatase Enzymes

Elisabeth Lambert,[‡] Barbara Chabut,[‡] Sylvie Chardon-Noblat,[⊥] Alain Deronzier,[⊥] Geneviève Chottard,[§] Azzedine Bousseksou,[†] Jean-Pierre Tuchagues,[†] Jean Laugier,[‡] Michel Bardet,[‡] and Jean-Marc Latour*[,‡]

Contribution from the CEA - Département de Recherche Fondamentale sur la Matière Condensée, SCIB-Laboratoire de Chimie de Coordination (URA CNRS 1194) CEA/Grenoble, 38054 Grenoble Cedex 9, France, Laboratoire de Chimie des Métaux de Transition, Université de Paris VI, Boîte 42, 75252 Paris Cedex 05, France, Laboratoire de Chimie de Coordination du CNRS, UPR 8241 liée par convention à l'Université Paul Sabatier et à l'Institut National Polytechnique de Toulouse, 205 Route de Narbonne, 31077 Toulouse Cedex, France, and Laboratoire d'Electrochimie Organique et de Photochimie Rédox (UMR 5630), Université Joseph Fourier, 38041 Grenoble Cedex, France

Received February 3, 1997[⊗]

Abstract: New asymmetrical ligands (H_2L) have been synthesized to provide both a bridging and a terminal phenolate to a pair of iron ions in order to mimic the binding of a single terminal tyrosinate at the diiron center of the purple acid phosphatases. H_2L1 is 2-[(bis(2-pyridylmethyl)amino)methyl]-6-[((2-pyridylmethyl)(2-phenol)amino)methyl]-4-methylphenol and $H_2L'1$ and H_2L2 are obtained by replacing the 2-phenol group by the 5-nitro-2-phenol and the 6-methyl-2-phenol residues, respectively. A series of mixed valence diiron complexes $[Fe^{II}Fe^{III}L(X)_2](Y)$ have been obtained where $(X)_2$ is the dianion of *m*-phenylenedipropionate or $(H_2PO_4)_2$ and Y = BPh_4 or PF_6 (L = L1, **1a** $(X)_2$ = mpdp, Y = BPh_4, **1b**: $(X)_2 = (OAc)_2$, Y = BPh_4, **1c**: $(X)_2 = (OBz)_2$, Y = BPh_4, **1d**: $(X)_2 = (H_2PO_4)_2$, Y = PF_6; L = L′1: **1′a** $(X)_2$ = mpdp, Y = BPh_4; L = L2: **2c**: $(X)_2 = (OBz)_2$, Y = BPh_4, **2d**: $(X)_2 = (H_2PO_4)_2$, Y = PF_6. Diferric complexes have been obtained also either by direct synthesis or by iodine oxidation of the mixed valence precursor (L = L1, **3a** $(X)_2$ = mpdp, Y = BPh_4, **3d**: $(X)_2 = (H_2PO_4)_2$, Y = PF_6; L = L2, **4d**: $(X)_2 = (H_2PO_4)_2$, Y = PF_6. Complex **1a** $[Fe^{II}Fe^{III}L(mpdp)](BPh_4)$ has been characterized by X-ray diffraction techniques. **1a** crystallizes in the monoclinic space group $P21/a$ with the following unit cell parameters: a = 22.038 (9) Å, b = 16.195 (8) Å, c = 16.536 (7) Å, β = 97.26 (1)°, Z = 4. The significant differences in the Fe−O bond lengths indicate that the metal centers are ordered. The complexes have been studied by electronic spectral, resonance Raman, magnetic susceptibility, Mössbauer, NMR, and electrochemical techniques. Mössbauer and NMR spectroscopies concur to probe that the valences of the mixed valence compounds are trapped in solution as well as in the solid state at room temperature. The electronic spectrum of the mixed-valence compounds are dominated by a charge transfer transition in the 400−600 nm domain which moves to the 550−660 nm range upon oxidation to the diferric state. In addition they exhibit a weak and broad intervalence transition close to 1100 nm. Electrochemical studies show that the systems exist in the three redox states $Fe^{II}Fe^{II}$ /$Fe^{II}Fe^{III}$ /$Fe^{III}Fe^{III}$. Moreover they show that the introduction of the terminal phenol group results in a thermodynamic destabilization of the diferrous state higher than the stabilization of the diferric state. An expanded stability domain of the mixed valence state is therefore observed which is probably due mostly to the asymmetry of the compounds. In addition a chemical destabilization of the reduced state of **1a**, **1c**, and **1′a** is observed. Comparison of the carboxylate and phosphate derivatives leads to attribute it to the partial dissociation in solution of the carboxylate oxygen *trans* to the phenolate. The latter feature bears an intrinsic resemblance with the dissociation of iron which is observed when purple acid phosphatases are reduced by dithionite. These studies clearly show the importance of tyrosine binding on the redox properties of the PAP enzymes. This questions the relationship of such a redox specificity with a hydrolytic function and raises the possibility that the latter may be redox regulated or that another (redox based) function is actually involved, possibly in line with the ability of the enzymes to react with peroxides.

The purple acid phosphatases[1] (PAP) belong to the class of iron oxo proteins characterized by a dinuclear oxo/hydroxo and carboxylato bridged active site.[2] Hemerythrin[3] (Hr) has long been considered the prototype of this class whose most prominent members are ribonucleotide reductase[4] (RNR) and methane monooxygenase[5] (MMO). These proteins are mostly

* Author for correspondence. Telefax (33) 04 76 88 50 90; e-mail: jlatour@cea.fr.
† Laboratoire de Chimie de Coordiantion du CNRS.
‡ SCIB-Laboratoire de Chimie de Coordination.
§ Université de Paris VI.
⊥ Université Joseph Fourier.
⊗ Abstract published in *Advance ACS Abstracts,* September 1, 1997.

(1) (a) Doi, K.; Antanaitis, B. L.; Aisen, P. *Struct. Bonding* **1988**, *70*, 1. (b) Vincent, J. B.; Olivier-Lilley, G. L.; Averill, B. A. *Chem. Rev.* **1990**, *90*,1447. (c) Que, L.; True, A. E. *Progr. Inorg. Chem.* **1990**, *38*, 97.
(2) Sanders-Loehr, J. In *Iron Carriers and Iron Proteins*; Loehr, T. M., Ed. VCH Publishers: New York, 1989; p 373.
(3) Stenkamp, R. E. *Chem. Rev.* **1994**, *94*, 715.
(4) Fontecave, M.; Nordlund, P.; Eklund, H.; Reichard, P. *Adv. Enzymol.* **1992**, *65*, 147.
(5) Lipscomb, J. D. *Ann. Rev. Microbiol.* **1994**, *48*, 371.

S0002-7863(97)00345-4 CCC: $14.00

involved in dioxygen transport and activation, and in such processes the oxidation level of the iron pair varies from Fe^{II}-Fe^{II} for the reduced active (*deoxy*) forms to $Fe^{III}Fe^{III}$ for the oxidized native (*met*) states. In addition mixed-valent forms $Fe^{II}Fe^{III}$ of the proteins can be generated *in vitro*. The X-ray structures of several forms of RNR[6] and MMO[7] have been determined very recently. They have revealed the diversity of the bridging pattern of the diiron unit (μ-oxo-bis-μ-carboxylato, μ-oxo-μ-carboxylato, μ-hydroxo-μ-carboxylato, bis-μ-carboxylato) as well as of the peripheral iron ligands which comprise only histidines in Hr and combinations of histidines and glutamates/aspartates in the other proteins.

The PAP enzymes differ from the other proteins of this class in several respects. *In vitro* they have been shown to catalyze phosphate hydrolysis with an optimum activity in the acidic range (pH ca. 5). However it has not been demonstrated that this is their biological function. PAP of various origins have been isolated but the more thoroughly studied originate from bovine spleen (BSPAP), pig allantoic fluid (uteroferrin, Uf), and red kidney bean (RKBPAP). The latter enzyme is peculiar in that its active site comprises a heterodinuclear FeZn unit. Its structure has been determined very recently.[8] Both metal atoms appear hexacoordinated and bridged by a hydroxide and a μ-1,1-carboxylate from an aspartate residue. The coordination sphere of the zinc ion comprises also two histidines, an asparagine, and a water molecule while that of the ferric ion includes a histidine, a tyrosinate, an aspartate, and a hydroxide. The structure of the diiron PAP enzymes is not known from X-ray crystallography; however, a wealth of spectroscopic studies involving EXAFS[9] and NMR[10] measurements have converged to the following structural hypothesis. In the mixed-valent state, the two iron atoms would be pentacoordinated and bridged by a hydroxide and a μ-1,3-carboxylate from an aspartate or a glutamate residue; the coordination sphere of the ferrous ion would include a histidine, a bidentate carboxylate, and a water molecule and that of the ferric ion a histidine, a tyrosinate, and a hydroxide. This spectroscopically effective model is consistent with the X-ray structure of the FeZn protein although minor differences do exist. Moreover, very recent sequence alignment studies have revealed a strong similarity of the metal binding sites in proteins of mammalian origin with the RKBPAP.[11]

The purple color ($\lambda_{max} \sim 550$ nm) of these proteins in the diferric state is due to a charge transfer transition from the tyrosinate group to the ferric ion. When they are reduced to the mixed-valent state they turn pink ($\lambda_{max} \sim 510$ nm), but the absorption retains the same intensity ($\epsilon \sim 4000\ M^{-1}\ cm^{-1}$). The latter feature indicates that the iron bound to the tyrosinate stays in the ferric state when the diiron center is reduced.

The Uf and BSPAP enzymes operate at the mixed-valence $Fe^{II}Fe^{III}$ state which is stable aerobically. Addition of phosphate however promotes the oxidation of the proteins to the diferric form which is inactive toward phosphate hydrolysis.[1] In contradistinction with the other proteins of the class the reduction of the diiron center does not produce a stable diferrous form.[12] Actually addition of dithionite to the oxidized protein leads to the rapid release of one iron atom ($t_{1/2} \sim$ 1mn), the second being released on a slower time scale ($t_{1/2} \sim$ 1h).

Scheme 1[a]

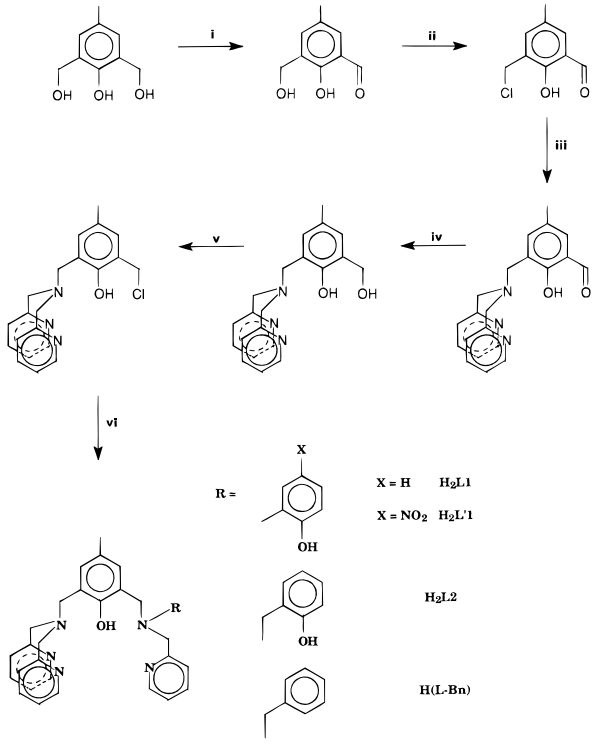

[a] **i**: MnO_2/toluene; ii: $SOCl_2/CH_2Cl_2$; iii: bis-picolylamine/NEt_3/THF; iv: $NaBH_4$/THF; v: $SOCl_2$; vi: substituted picolylamine/NEt_3/THF.

Modeling studies of the PAP enzymes have focused on two specific features: the presence of the tyrosinate ligand and the binding of oxo anions (phosphate, molybdate, arsenate). A series of potential models of the PAP active site have been elaborated from the phenol based dinucleating tetrapyridyl ligand (HLPy4) introduced by Suzuki *et al.*[13] and Que *et al.*[14] and the analogous tetraimidazole ligand (HLIm4) from Buchanan[15] and tetrabenzimidazole ligand (HLBzIm4) from Suzuki.[16] Several complexes have been isolated which incorporate diphenylphosphate bridges.[17,18] In the last couple of years several groups have reported the synthesis and some properties of diiron complexes of related ligands ($H_3LPy_2PhO_2$ and $H_3LIm_2PhO_2$) where two nitrogen donors have been replaced with two phenols.[19−21] In these derivatives, there is one phenolate per iron atom instead of one phenolate per iron pair, the ratio found in the proteins.

In this article we describe the synthesis of asymmetrical ligands obtained upon substitution of one picolyl group by a phenol in Suzuki's tetrapyridyl ligand[13] (Scheme 1). These

(6) (a) Nordlund, P.; Sjöberg, B.-M.; Eklund, H. *Nature* **1990**, *345*, 593. (b) Åberg, A.; Nordlund, P.; Eklund, H. *Nature* **1993**, *361*, 276. (c) Nordlund, P.; Eklund, H. *J. Mol. Biol.* **1993**, *232*, 123.

(7) (a) Rosenzweig, A. C.; Frederick, C. A.; Lippard, S. J.; Nordlund, P. *Nature* **1993**, *366*, 537. (b) Rosenzweig, A. C.; Nordlund, P.; Takahara, P. M.; Frederick, C. A.; Lippard, S. J. *Chem. Biol.* **1995**, *2*, 409.

(8) Sträter, N.; Klabunde, T.; Tucker, P.; Witzel, H.; Krebs, B. *Science* **1995**, *268*, 1489.

(9) True, A. E.; Scarrow, R. C.; Randall, C. R.; Holz, R. C.; Que, L., Jr. *J. Am. Chem. Soc.* **1993**, *115*, 4246.

(10) (a) Scarrow, R. C.; Pyrz, J. W.; Que, L., Jr. *J. Am. Chem. Soc.* **1990**, *112*, 657. (b) Wang, Z.; Ming, L. J.; Que, L.; Vincent, J. B.; Crowder, M. W.; Averill, B. A. *Biochemistry* **1992**, *31*, 5263.

(11) Klabunde, T.; Sträter, N.; Krebs, B.; Witzel, H. *FEBS Lett.* **1995**, *367*, 56.

(12) Keough, D. T.; Dionysius, D. A.; de Jersey, J. B.; Zerner, *Biochem. Biophys. Res. Commun.*, **1980**, *94*, 600.

(13) Suzuki, M.; Uehara, A.; Oshio, H.; Endo, K.; Yanaga, M.; Kida S.; Saito, K. *Bull. Chem. Soc. Jpn.* **1987**, *60*, 3547.

(14) Borovik, A. S.; Papaefthymiou, V.; Taylor, L. F.; Anderson, O. P.; Que, L. *J. Am. Chem. Soc.* **1989**, *111*, 6183.

(15) Mashuta, M.; Webb, R. J.; McCusker, J. K.; Schmitt, E. A.; Oberhausen, K. J.; Richardson, J. F.; Buchanan, R. M.; Hendrickson, D. N. *J. Am. Chem. Soc.* **1992**, *114*, 3815.

(16) Suzuki, M.; Oshio, H.; Uehara, A.; Endo, K.; Yanaga, M.; Kida, S.; Saito, K. *Bull. Chem. Soc. Jpn.* **1988**, *61*, 3907.

(17) Schepers, K.; Bremer, B.; Krebs, B.; Henkel, G.; Althaus, E.; Mosel, B.; Müller-Warmuth, W. *Angew. Chem.* **1990**, *29*, 531.

(18) Ming, L.-J.; Jang, H. G.; Que, L. *Inorg. Chem.* **1992**, *31*, 359.

ligands have been used to prepare the first asymmetrical diiron-(II,III) complexes which mimic the coordination of the tyrosinate at the PAP active site.[22] While this work was nearing completion Neves *et al.* reported the synthesis and some properties of a similar diiron complex of ligand H_2L2.[23] The asymmetry of the environment introduced by the single terminal phenolate influences drastically the redox properties of the diiron site: the strong destabilization of the diferrous state and the less pronounced stabilization of the diferric one lead to an enlarged stability domain for the mixed valence state. The electrochemical study of various carboxylate and phosphate bridged derivatives provides some clues on the major factors which affect the redox behavior of the complexes. In addition, we found that a chemical process follows the formation of the diferrous derivative of ligand H_2L1; electrochemical and spectroscopic evidences strongly suggest that this process is the decoordination of a carboxylate bridge, a process reminiscent of the enzyme behavior in the presence of dithionite.

Experimental Section

Materials. 2,6-Bis(hydroxymethyl)-4-methylphenol, salicylaldehyde, 2-aminophenol, 2-amino-4-nitrophenol, 2-aminomethylpyridine, and 2-picolyl chloride hydrochloride were obtained from Aldrich Chemical Co. Sodium 1,3-*m*-benzenedipropionate was prepared according to the literature procedure.[24] THF and triethylamine were distilled under argon on Na/benzophenone and calcium hydride, respectively. Acetonitrile (HPLC grade S) for electrochemistry was obtained from Rathburn, stored under inert atmosphere, and used without further purification. Tetrabutylammonium perchlorate (Fluka purum) was recrystallized in ethyle acetate/cyclohexane. All other reagents were of reagent grade quality and used as received.

Syntheses. *N*-(2-hydroxyphenyl)-*N*-(2-pyridylmethyl)amine. Three grams (2.75×10^{-2} mol) of *o*-aminophenol and 2.94 g (2.75×10^{-2} mol) of pyridine-2-carboxaldehyde were dissolved in 150 mL of methanol. The solution was stirred 2 h at room temperature. After addition of 1.04 g (2.75×10^{-2} mol) of sodium borohydride stirring was maintained for 1 h. After evaporation of methanol, the solid residue was dissolved in dichloromethane, washed with an aqueous solution of ammonium chloride, and dried over Na_2SO_4. Evaporation of the solvent and recrystallization of the product in methanol produced 2.75 g of the amine (yield 50%). Mass spectrometry (CI, NH_3): $M + H^+ = 201$.

An identical procedure was used to prepare *N*-(2-hydroxy-5-nitrophenyl)-*N*-(2-pyridylmethyl)amine.

***N*-(2-Hydroxybenzyl)-*N*-(2-pyridylmethyl)amine.** This amine was prepared similarly, but after evaporation of the solvent it was transformed into its hydrochloride salt by treatment with a 37% hydrogen chloride aqueous solution. After recrystallization in methanol, the hydrochloride was isolated in a 90% yield. Mass spectrometry (CI, NH_3): $M + H^+ = 215$.

2-(Hydroxymethyl)-6-carbaldehyde-4-methylphenol, I. Fifteen grams (8.9×10^{-2} mol) of 2,6-bis(hydroxymethyl)-4-methylphenol and 19.5 g of manganese dioxide were stirred in 3 L of toluene at room temperature for 4 days. MnO_2 was filtered off, and evaporation of toluene gave 9.3 g of the crude product. Recrystallization in toluene (10 mL/g) afforded 7.4 g of I as a white powder (yield 50%). Mass spectrometry: (CI, NH_3): $M + NH_4^+ = 184$.

2-(Chloromethyl)-6-carbaldehyde-4-methylphenol, II. I (7.49 g, 4.3×10^{-2} mol) was suspended in 12 mL of dichloromethane. Upon adding dropwise a solution of 8 mL of thionyl chloride in 12 mL of dichloromethane a clear bright yellow solution was obtained. After stirring for 1 hour the solvent and $SOCl_2$ were evaporated off with a water pump. The residue was dissolved in 20 mL of dichloromethane, and the solution diluted with 20 mL of hexane. Slow concentration under reduced pressure induced the crystallization of **II** as white needles which were collected by filtration and washed with hexane. Concentration of the filtrate gave a second crop. (Yield 8.2 g, 99%) mass spectrometry: (CI, NH_3): $M + NH_4^+ - HCl = 166$.

2-(*N*,*N*-Bis(2-methylpyridyl)aminomethyl)-6-carbaldehyde-4-methylphenol, III. Bis-picolylamine (5.2 g, 2.6×10^{-2} mol) and 5.6 g (2.99×10^{-2} mol) of **II** were dissolved in 150 mL of THF and 13.4 mL (10^{-1} mol) of triethylamine. Spontaneous precipitation of $Et_3N^+Cl^-$ was observed, and the solution turned lemon yellow. After stirring overnight at room temperature, the precipitate was removed by filtration, and the solution was evaporated out leaving 10 g of crude product. The product was dissolved in a 37% HCl aqueous solution and the solution was extracted with dichloromethane to eliminate the excess of **II**. After evaporation of the water, the product was dissolved in a saturated Na_2CO_3 solution and extracted with dichloromethane. After drying over Na_2SO_4 and evaporation of the solvent 8 g of **III** was obtained as a greenish oil which crystallized slowly upon standing (yield 90% with respect to bis-picolylamine). Mass spectrometry: (CI, NH_3): $M + H^+ = 348$.

2-(*N*,*N*-Bis(2-methylpyridyl)aminomethyl)-6-(hydroxymethyl)-4-methylphenol, IV. Four grams (1.15×10^{-2} mol) of **III** were dissolved in methanol and treated by 1.2 g (3.17×10^{-2} mol) of sodium borohydride. Spontaneous bleaching of the solution and hydrogen evolution were observed. The solution was stirred 15 mn at room temperature and 30 mn at reflux. It was then acidified to pH 2−3 with hydrogen chloride to eliminate boron complexes which had formed and precipitated out. After filtration the solvent was evaporated, and the product redissolved in an aqueous $NaHCO_3$ solution and extracted with dichloromethane. Drying over Na_2SO_4 and evaporation of the solvent afforded 4.0 g of **IV** (yield ca. 100%).

2-(*N*,*N*-Bis(2-methylpyridyl)aminomethyl)-6-(chloromethyl)-4-methylphenol, V. One gram (2.87×10^{-3} mol) of **IV** was dissolved in a minimum of freshly distilled thionyl chloride (10 mL). The solution was stirred at room temperature for 3 h. $SOCl_2$ was then distilled under reduced pressure at 30−40 °C, and the product was washed several times with hexane and dichloromethane (yield ca. 100%). Mass spectrometry (FAB^+, *m*-nitrobenzyl alcohol): $M + H^+ = 368$.

2-(*N*,*N*-Bis(2-methylpyridyl)aminomethyl)-6-(*N*-(2-hydroxyphenyl)-*N*-(2-pyridylmethyl)aminomethyl)-4-methylphenol, H_2L1. V (5.55 g, 1.37×10^{-2} mol) and 2.75 g (1.37×10^{-2} mol) of (*N*-(2-hydroxyphenyl)-*N*-(2-pyridylmethyl)amine were dissolved in 150 mL of THF. Eleven grams of triethylamine (1.09×10^{-1} mol) were then added, and the solution was stirred for 24 h at room temperature. Evaporation of the solvent produced an oil which was dissolved in dichloromethane, washed with a pH 7 buffer, and dried over Na_2SO_4. Evaporation of the solvent gave an oily product which was diluted with a minimum amount of methanol. After standing at 4 °C ligand H_2L1 precipitated out as a white powder (3.3 g, yield 45%). Mass spectrometry (FAB^+, *m*-nitrobenzyl alcohol): $M + H^+ = 532$. NMR ^1H (CD_3CDO), δ (ppm): 2.1 (s, 3H, CH_3); 3.73 (s, 2H, CH_2); 3.84 (s, 4H, CH_2); 4.14 (s, 2H, CH_2); 4.22 (s, 2H, CH_2); 6.65 (dt, 1H, CH-12); 6.8 and 6.92 (2d, 2H, CH-19 and CH-21); 6.85 (dd, 1H, CH-14); 6.87 (dt, 1H, CH-13); 7.00 (td, 1H, CH-5); 7.15 (d, 1H, CH-3); 7.22 (dd, 1H, CH-11); 7.25 (dt, 2H, CH-29); 7.35 (dt, 1H, CH-4); 7.41 (d, 2H, CH-31); 7.70 (dt, 2H, CH-30); 8.35 (ddd, 1H, CH-6); 8.60 (ddd, 2H, CH-28). RMN ^{13}C (CD_3CDO), δ (ppm): 18.87 (CH_3); 54.60 (CH_2); 55.66 (CH_2-7); 57.31 (CH_2); 57.86 (CH_2-25); 114.72 (CH-14); 118.14 (CH-12); 121.04 (CH-5); 121.33 (C26); 121.56 (CH-29); 122.30 (CH-31); 123.62 (C9); 124.23 (CH-13); 126.4 (C20); 129.56 and 130.58 (CH-19 and CH-21); 135.43 (CH-4);136.08 (CH-30); 137.81 (C10); 147.57 (CH-6); 148.14 (CH-28); 152.66 (C16); 153.02 (C18); 157.64 (C26); 158.99 (C2); 204.71 (C17).

An identical procedure was used to prepare $H_2L'1$ from (*N*-(2-hydroxy-5-nitrophenyl)-*N*-(2-pyridylmethyl) amine.

(19) (a) Neves, A.; Erthal, S. M. D.; Drago, V.; Griesar, K.; Haase, W. *Inorg. Chim. Acta* **1992**, *197*, 121. (b) Neves, A.; de Brito, M. A.; Vencato, I.; Drago, V.; Griesar, K.; Haase, W. *Inorg. Chem.* **1995**, *35*, 2360.

(20) Krebs, B.; Schepers, K.; Bremer, B.; Henkel, G.; Althaus, E.; Müller-Warmuth, W.; Griesar, K.; Haase, W. *Inorg. Chem.* **1994**, *33*, 1907.

(21) Nie, H.; Aubin, S. M. J.; Mashuta, M. S.; Wu, C.-C.; Richardson, J. F.; Hendrickson, D. N.; Buchanan, R. B. *Inorg. Chem.* **1995**, *34*, 2382.

(22) Bernard, E.; Moneta, W.; Laugier, J.; Chardon-Noblat, S.; Deronzier, A.; Tuchagues, J.-P.; Latour, J.-M. *Angew. Chem., Int. Ed. Engl.* **1994**, *33*, 887.

(23) Neves, A.; de Brito, M. A.; Drago, V.; Griesar, K.; Haase, W. *Inorg. Chim. Acta* **1995**, *237*, 131.

(24) Beer, R. H.; Tolman, W. B.; Bott, S. G. Lippard, S. J. *Inorg. Chem.* **1989**, *28*, 557.

2-(*N*,*N*-Bis(2-methylpyridyl)aminomethyl)-6-(*N*-(2-hydroxybenzyl)-*N*-(2-pyridylmethyl)aminomethyl)-4-methylphenol, H_2L2. Ligand H_2L2 was prepared similarly in a 50% yield. Mass spectrometry (FAB^+, *m*-nitrobenzyl alcohol): $M + H^+ = 546$.

NMR ^{1}H (MeOD), δ (ppm): 2.16 (s, 3H, CH_3); 3.70 (s, 2H, CH_2); 3.71 (s, 2H, CH_2); 3.77 (s, 2H, CH_2); 3.78 (s, 2H, CH_2); 3.80 (s, 4H, CH_2); 6.72 (dd, 1H, CH-15); 6.74 (dt, 1H, CH-13); 6.85 (s, 2H, CH-20 and CH-22); 7.07 (dd, 1H, CH-12); 7.09 (dt, 1H, CH-14); 7.20 (ddd, 3H, CH-5 and CH-30); 7.39 (dd, 1H, CH-3); 7.49 (dd, 2H, CH-32); 7.62 (dt, 1H, CH-4); 7.68 (dt, 2H, CH-31); 8.42 (ddd, 1H, CH-6); 8.46 (ddd, 2H, CH-29). RMN ^{13}C (CD_2Cl_2), δ (ppm): 20.64 (CH_3); 57.04 (CH_2-16 and CH_2-24); 57.49 (CH_2-9); 59.46 (CH_2-7); 59.57 (CH_2-26); 116.5 (CH-15); 119.21 (CH-13); 122.56 (CH-3 and CH-32); 123.54 (C10); 123.64 and 123.94 (CH-5 and CH-30); 127.79 (C21); 129.27 (CH-14); 130.05 (CH-12); 130.86 and 131.7 (CH-20 and CH-22); 136.82 and 137.03 (CH-4 and CH-31); 149 (CH-6 and CH-29); 154.64 (C17); 158.45 (C19); 158.68 (C27); 159.07 (C2).

$[Fe^{II}Fe^{III}(L1)(mpdp)](BPh_4)$, 1a. A dark brown solution was obtained when 1.52 g (3.76×10^{-3} mol) of $Fe(NO_3)_3 \cdot 9H_2O$ in 100 mL of methanol was added to a solution of 1 g (1.88×10^{-3} mol) of H_2L1 in 100 mL of methanol. Sodium 1,3-benzenedipropionate (Na_2-mpdp) (550 mg, 2.07×10^{-3} mol) in 100 mL of methanol was then added. After the reaction mixture was stirred for 1 h, excess sodium tetraphenylborate BPh_4 (4 equiv, 2.6 g) was added to precipitate the desired complex (1.25 g, yield 56%) as a brown powder. Recrystallization in an acetonitrile/ethanol mixture afforded black needles of **1a** of X-ray quality.

The other complexes of H_2L1 were obtained in the same way by replacing Na_2mpdp by sodium acetate (**1b**), sodium benzoate (**1c**), and sodium diphenylphosphate (**1d**). They were obtained with similar yields: **1b**, 54%; **1c**, 60%; **1d**, 47%.

Mass spectrometry (FAB^+, *m*-nitrobenzyl alcohol): **1a:** $[Fe^{II}Fe^{III}(L1)(mpdp)]^+$ $M = 861$. **1b**: $[Fe^{II}Fe^{III}(L1)(OAc)_2]^+$ $M = 759$. **1c:** $[Fe^{II}Fe^{III}(L1)(OBz)_2]^+$ $M = 883$. **1d**: $[Fe^{II}Fe^{III}(L1)(dpp)_2]^+$ $M = 1139$. **1′a**: $[Fe^{II}Fe^{III}(L'1)(mpdp)]^+$ $M = 906$.

$[Fe^{II}Fe^{III}(L2)(OBz)_2](BPh_4)$, 2c. A dark blue solution was obtained when 74 mg (1.83×10^{-4} mol) of $Fe(NO_3)_3 \cdot 9H_2O$ in 10 mL of methanol was added to a solution of 50 mg (9.17×10^{-5} mol) of H_2-L2 in 30 mL of methanol. Sodium benzoate (26 mg, 1.83×10^{-4} mol) in 30 mL of methanol was then added. After the reaction mixture was stirred for 1 h, excess sodium tetraphenylborate BPh_4 (4 equiv, 126 mg) was added to precipitate the desired complex (61 mg yield 55%) as a dark blue powder. Mass spectrometry (FAB^+, *m*-nitrobenzyl alcohol): $[Fe^{III}Fe^{III}(L2)(OBz)_2]^+$ $M = 897$.

$[Fe^{II}Fe^{III}(L2)(dpp)_2](PF_6)$, 2d. A dark blue solution was obtained when 741 mg (1.83×10^{-3} mol) of $Fe(NO_3)_3 \cdot 9H_2O$ in 100 mL of methanol was added to a solution of 500 mg (9.17×10^{-4} mol) of H_2L2 in 100 mL of methanol. Sodium diphenylphosphate (Nadpp) (500 mg, 1.83×10^{-3} mol) and 91 mg (4.6×10^{-4} mol) of sodium ascorbate in 100 mL of methanol were then added. After the reaction mixture was stirred for 1 h, excess sodium hexafluorophosphate $NaPF_6$ (4 equiv, 616 mg) was added to precipitate the desired complex (825 mg, yield 62%) as a dark blue powder. Mass spectrometry (FAB^+, *m*-nitrobenzyl alcohol): $[Fe^{II}Fe^{III}(L2)(dpp)_2]^+$ $M = 1153$.

$[Fe^{III}Fe^{III}(L1)(mpdp)](I_3)(BPh_4)$, 3a. 1a (50 mg, 4.23×10^{-5} mol) was dissolved in 50 mL of acetonitrile. The addition of 16 mg (1.5 equiv) of iodine caused an immediate color change from brown to green. Addition of methanol induced the precipitation of complex **3a** (35 mg, yield 70%). Mass spectrometry (FAB^+, *m*-nitrobenzyl alcohol): $[Fe^{III}$-$Fe^{III}(L1)(mpdp)]^+$ M = 861.

$[Fe^{III}Fe^{III}(L1)(dpp)_2](I_3)(BPh_4)$, 3d. Iodine (29 mg, 1.5 equiv) was added to a solution of 110 mg (7.55×10^{-5} mol) of **1d** in 50 mL of acetonitrile. Addition of methanol induced the precipitation of complex **3d** (80 mg, yield 58 %). Mass spectrometry (FAB^+, *m*-nitrobenzyl alcohol): $[Fe^{III}Fe^{III}(L1)(dpp)_2]^+$ M = 1139.

$[Fe^{III}Fe^{III}(L2)(dpp)_2](PF_6)_2$, 4d. An intense blue solution was obtained when 741 mg (1.83×10^{-3} mol) of $Fe(NO_3)_3 \cdot 9H_2O$ in 100 mL of methanol was added to a solution of 500 mg (9.17×10^{-4} mol) of H_2L2 in 100 mL of methanol. Sodium diphenylphosphate (Nadpp) (500 mg, 1.83×10^{-3} mol) in 100 mL of methanol was then added. After the reaction mixture was stirred for 1 h, excess sodium hexafluorophosphate $NaPF_6$ (4 equiv, 616 mg) was added to precipitate the desired complex (1.15 g, yield 98%) as a dark blue powder. Mass spectrometry (FAB^+, *m*-nitrobenzyl alcohol): $[Fe^{III}Fe^{III}(L2)(dpp)_2]^{2+}$ $M = 1153$.

X-ray Crystallography. Intensity data were collected on an Enraf Nonius P4 diffractometer (Mo Kα, $\lambda = 0.71073$ Å) by using the ω scan mode to a maximum 2θ value of 55° and a variable scan rate (0.33−2.7°/mn). Two test reflections (081 and 009) were measured every 200 data points. No significant variation of their intensities were noted during collection of the data. Therefore no extinction or absorption correction were applied. The structure was solved by direct methods and the remaining non-hydrogen atoms located by combination of full-matrix least-squares refinement cycles and Fourier syntheses. The hydrogen atoms were located at calculated positions and refined isotropically. All non-hydrogen atoms were refined anisotropically. Final atomic coordinates and isotropic thermal parameters are listed in Table SM1 of the Supporting Information.

Physicochemical Studies. Mass spectra were obtained on a VG-ZAB-SEQ apparatus operating in the positive FAB mode. Elemental analyses were performed by the Service Central d'Analyse of the Centre National de la Recherche Scientifique. All compounds gave satisfactory elemental analyses.

Electronic absorption spectra were recorded on a Lambda 9 Perkin Elmer spectrometer in methanol and acetonitrile. The resonance Raman spectra were obtained on a J.Y. U1000 double monochromator, equipped with an AsGa photomultiplier and photon counting electronics. Excitation wavelengths of 80 mW power (reduced to 30 mW for the violet lines) from Ar^+ and Kr^+ lasers were used. The mechanical slit width was set to 400 μm, so that the spectral slit width varied from 2 cm^{-1} at 676.4 nm to 6 cm^{-1} at 406.7 nm. The complexes were studied in the solid state, as powders compressed on a rotating disc as well as in solution (3 mM in acetonitrile, rotating cell). The 1375 cm^{-1} band of acetonitrile was used to measure the relative intensity (based on peak heigths) of the high frequency bands, at various wavelengths. For the 620 cm^{-1} band, the 920 cm^{-1} band of acetonitrile was used as a standard.

Magnetization experiments were done with a SHE 900 and a MPMS Quantum Design SQUID magnetometer operating at 0.5−5 T in the 2−300 K temperature range. The samples as microcrystalline powders (ca. 20 mg) were contained in a kel F bucket which had been calibrated independently at the same field and temperatures. Diamagnetic contributions were calculated from tabulated Pascal's constants.[25]

Mössbauer measurements were obtained on a constant-acceleration conventional spectrometer with a 25 mCi source of ^{57}Co(Rh matrix). Isomer shift values (δ) throughout the paper are given with respect to metallic iron at room temperature. The absorber was a sample of 120 mg of microcrystalline powder enclosed in a 2 cm diameter cylindrical plastic sample-holder, the size of which had been determined to optimize the absorption. Variable-temperature spectra were obtained in the 300−4.2 K range, by using a MD 306 Oxford cryostat, the thermal scanning being monitored by an Oxford ITC4 servocontrol device (±0.1 K accuracy). A least-squares computer program[26] was used to fit the Mössbauer parameters and determine their standard deviations of statistical origin (given in parentheses).

A Varian UNITY 400 spectrometer with a 5 mm indirect detection, operating at 400 MHz for the proton, was used for collection of both 1D and 2D ^{1}H NMR spectra. The 1 D spectra were obtained with a 90° pulse. The use of a fast analogic-digital convertor was necessary to cover the full ^{1}H chemical shift range (up to 600 ppm). Spectra for the nonselective T_1 experiments were acquired using the classical inversion-recovery pulse sequence. Due to the large chemical shift range, the carrier frequency was set to different positions to ensure the validity of the measurements. Each T_1 experiment involved at least ten different values for the incremental delay. Reported T_1 values represent the average of three different determinations and have an accuracy better than 5%.

Owing to the very short T_1, T_2, and the large chemical shift range, only the classical COSY displayed in magnitude mode yielded useful correlations. In order to decrease the t_1 noise arising from signals of

(25) O'Connor, C. J. *Prog. Inorg. Chem.* **1982**, *29*, 203.

(26) Varret, F. *Proceedings of the International Conference on Mössbauer Effect Applications*; Jaipur, India, 1981; Indian National Science Academy: New Delhi, 1982.

the tetraphenylborate protons which have much longer T_1 than those of the cation, we applied a 180° pulse before the COSY sequence itself, followed by a 300 ms delay (WEFT sequence). The other parameters used to collect the 2D spectra are 2048 points in t_2 and 1024 blocks in t_1. The number of transients was set at 1024. The relaxation delay was set to 0.7 s when the WEFT sequence was used and 0.1 s in other cases. The time domain data were processed using 0° phase-shifted sine-bell-squared window functions in both dimensions and zero-filled to a final size of 2048*2048. Steady state 1D ^{1}H NOE measurements were obtained by using 10−300 ms irradiation time for the different signals of interest. Control spectra were recorded with an off resonance irradiation. The NOE difference spectra were obtained by computer subtraction of each spectrum with the control. Spectra were accumulated by blocks of 128 transients up to 3600 in an interleaved manner. In order to increase the intensity of the NOE (negative regime) the spectra were recorded at 240 K.

Electrochemical measurements were done with the usual three electrode system driven by a potentiostat/galvanostat PAR 273. The reference electrode consisted in a silver wire immersed in a 10^{-2} M solution of silver nitrate in an acetonitrile solution 10^{-1}M in tetrabutylammonium perchlorate. The auxiliary electrode was a platinum wire immersed in an acetonitrile solution 10^{-1}M in tetrabutylammonium perchlorate. Voltamperometric measurements were done with a rotating electrode (Tacussel EDI) equipped with a disk of vitreous carbon 2 mm in diameter. For cyclic voltammetry the working electrode was a disk of platinum or vitreous carbon with a diameter of 3 mm. A platinum plate of area 5 cm^2 was used for exhaustive electrolyses. The experiments were performed in a drybox (Jaram) with a dioxygen content lower than 5 ppm. The electrochemical experiments were also followed by electronic absorption spectroscopy using a Hewlett-Packard 8452A diode array spectrophotometer. Initial and electrolyzed solutions were transferred to a conventional cuvette cell within the drybox. The cell was inserted into the optical translator connected to the spectrophotometer through a fiber optic system (Photonics Spectrofip system).

Results

Syntheses of the Ligands. The synthesis of the asymmetrical ligands bearing a terminal phenolate in a single lateral branch is illustrated in Scheme 1. The introduction of the asymmetry, the key step in the synthesis, is realized in the first step through oxidation of a single hydroxymethyl group by manganese dioxide. Subsequent chlorination and alkylation of (bis-picolyl)-amine affords the tris-amine branch. Borohydride reduction of the carbonyl regenerates the hydroxymethyl group which is similarly chlorinated for alkylation of a second amine different from the first one. This procedure is quite general and affords the desired ligands in gram quantities with an overall yield of ca. 23%. Two different amines were used in the present study 2-[(bis-2-picolyl)amino]phenol and 2-[(bis-2-picolyl)amino]-methyl phenol leading, respectively, to ligands H_2L1 and H_2L2. Alternatively the lateral phenols can be replaced by a noncoordinating group (e.g., benzyl).[27] A similar multistep procedure was recently reported[28] which differs in the initial mode of introduction of the ligand asymmetry. On the other hand, Neves *et al*. obtained H_2L2 by a statistical synthesis from 2,6-bis-(chloromethyl)-4-methylphenol.[23]

Syntheses of the Complexes.[29] Reaction of the ligand H_2-L1 with $Fe(NO_3)_3{\cdot}9H_2O$ and sodium 1,3-benzenedipropionate (Na_2mpdp) affords a violet precipitate of **1a** after addition of sodium tetraphenylborate. Recrystallization in acetonitrile gives crystals suitable to an X-ray diffraction determination. Elemental analysis and various spectroscopic methods (see below) show that **1a** is the mixed-valent complex $[Fe^{II}Fe^{III}(L1)(mpdp)](BPh_4)$. A similar procedure has been used to prepare analogous complexes with various carboxylate bridges (acetate: **1b**, benzoate: **1c**) and diphenylphosphate **1d**. Electrochemical studies (see below) show that these complexes can be oxidized at low positive potentials (ca. 0.25 V_{NHE}). This property has been used to prepare the corresponding diferric derivatives by oxidation of **1a** and **1d** with iodine. Spectrophotometric titration showed that 1.5 equiv of I_2 were required pointing to a one-electron oxidation:

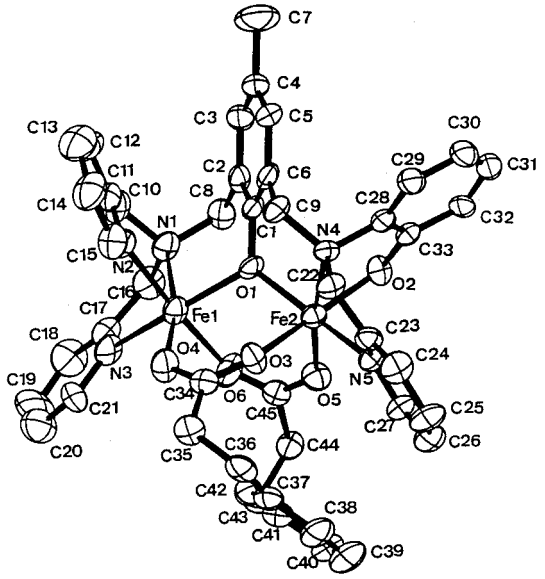

Figure 1. Structure of the cation of **1a**.

$$[Fe^{II}Fe^{III}(L1)(X)_2](BPh_4) + {}^3/_2I_2 \rightarrow [Fe^{III}Fe^{III}(L1)(X)_2](I_3)(BPh_4)$$

$$(X)_2 = \text{mpdp or } (dpp)_2$$

The corresponding complexes **3a** ($(X)_2$ = mpdp) and **3d** ($(X)_2$ = $(dpp)_2$) were characterized by elemental analyses, mass spectrometry and spectroscopic methods.

Surprisingly ^{1}H-NMR shows that the reaction of H_2L2 with $Fe(NO_3)_3{\cdot}9H_2O$ and Na_2mpdp does not produce a single mixed-valent complex as for H_2L1 but a mixture of two such species which have not been identified. Aliphatic carboxylates (e.g., acetate, propionate, pivalate) and even formiate behave in the same way. This behavior may be related to the strong donating ability of the terminal phenolate (see below). A pure dicarboxylate derivative could be isolated only with the less electron donating sodium benzoate: $[Fe^{II}Fe^{III}(L2)(OBz)_2](BPh_4)$, **2c**. It is noteworthy that Neves *et al*. could isolate the acetate derivative **2b** from reaction of H_2L2 with ferrous perchlorate.[23] When sodium diphenylphosphate is used the diferric complex is obtained from the reaction mixture upon addition of sodium hexafluorophosphate: $[Fe^{III}Fe^{III}(L2)(dpp)_2](PF_6)_2$, **4d**. This complex can be reduced easily with sodium ascorbate to afford the corresponding mixed-valent compound: $[Fe^{II}Fe^{III}(L2)(dpp)_2](PF_6)$, **2d**. All complexes have been characterized by elemental analyses, mass spectrometry and spectroscopic methods.

X-ray Structure of $[Fe_2(L1)(mpdp)](BPh_4)$, 1a. Crystals of **1a** consist in discrete cations $[Fe_2(L1)(mpdp)]^+$and tetraphenylborate anions. The structure of the cation is illustrated in Figure 1. The crystal parameters are listed in Table 1, and

(27) Kanda, W.; Moneta, W.; Bardet, M.; Bernard, E.; Debaecker, N.; Laugier, J.; Bousseksou, A.; Chardon-Noblat, S.; Latour, J.-M. *Angew. Chem., Int. Ed. Engl.* **1995**, *34*, 588.

(28) (a) Belle,C.; Gellon, G.; Scheer, C.; Pierre, J. L. *Tetrahedron Lett.* **1994**, *35*, 7019. (b) Belle, C.; Gautier-Luneau, I.; Pierre, J. L.; Scheer, C. *Inorg. Chem.* **1996**, *35*, 3706.

(29) The diiron complexes are labeled as follows: those of H_2L1 are indicated by odd numbers, those of H_2L2 by even ones; 1 and 2 refer to mixed-valent compounds, 3 and 4 to diferric ones. Each alphabetical index is associated to a specific oxoanion bridge, a: mpdp, b: acetate, c: benzoate, d: diphenylphosphate.

Table 1. Summary of Crystal Data and Structure Refinement for Complex **1a**

formula	$C_{69}H_{63}N_5O_6BFe_2$
molecular weight	1180.8
crystal dimensions, mm	0.30*0.35*0.20
space group	*P*21/*a*, monoclinic
a, Å	22.038(9)
b, Å	16.195(8)
c, Å	16.536(7)
β, °	97.26
V, Å^3	5854.5
Z	4
T, K	298
ρ_{calcd}, g·cm^{-3}	1.34
μ, mm^{-1}	0.55
index ranges	$-28 < h < 28$, $0 < k < 21$, $0 < l < 21$
total reflections	14375
unique data ($F > 4*\sigma(F)$)	6583
parameters refined	790
R	0.052
Rw (weight = $1/(\sigma(F)^2)$	0.042

Table 2. Selected Interatomic Distances (Å) and Angles (deg) for Complex **1a**

Fe1−O1	2.073	Fe2−O1	1.949
Fe1−O4	2.037	Fe2−O2	1.936
Fe1−O6	2.178	Fe2−O3	2.053
Fe1−N1	2.238	Fe2−O5	1.965
Fe1−N2	2.170	Fe2−N4	2.244
Fe1−N3	2.118	Fe2−N5	2.147
Fe1−Fe2	3.417		
O1−Fe1−N1	88.1	O1−Fe2−N4	88.6
O1−Fe1−N2	91.5	O1−Fe2−N5	160.5
O1−Fe1−N3	160.6	O1−Fe2−O2	97.0
O1−Fe1−O4	100.9	O1−Fe2−O3	89.0
O1−Fe1−O6	86.5	O1−Fe2−O5	100.4
N1−Fe1−N2	78.6	N4−Fe2−N5	75.6
N1−Fe1−N3	77.8	N4−Fe2−O2	80.2
N1−Fe1− O4	167.3	N4−Fe2−O3	88.0
N1−Fe1− O6	95.2	N4−Fe2−O5	170.2
N2−Fe1−N3	98.6	N5−Fe2−O2	91.4
N2−Fe1− O4	92.1	N5−Fe2−O3	79.4
N2−Fe1− O6	173.5	N5−Fe2−O5	96.4
N3−Fe1−O4	95.3	O2−Fe2−O3	166.6
N3−Fe1−O6	81.6	O2−Fe2−O5	94.6
O4−Fe1−O6	94.3	O3−Fe2−O5	96.1
Fe1−O1−Fe2	116.4		

important distances and angles are summarized in Table 2. The two iron atoms are bridged by the phenolate oxygen O1 and the two carboxylate groups of the mpdp ligand. The coordination of Fe1 is complemented by the three nitrogen atoms N1, N2, and N3, of the bispicolylamine branch. The overall N_3O_3 coordination around Fe1 corresponds to a rhombically distorted octahedron. The coordination of Fe2 is complemented by the two nitrogen atoms N4 and N5, from the tertiary amine and the pyridine group and the O5 oxygen of the terminal phenolate. The overall N_2O_4 coordination around Fe2 is best described as a rhombically distorted octahedron. It is worth noting that the distances from the pyridine nitrogens to Fe1 are rather similar 2.118 vs 2.170 Å and moreover the one *trans* to the bridging phenolate is shorter, therefore ruling out any strong trans effect of this ligand in the complex. The longest bond is the one to the tertiary amine as is also the case for Fe2. The Fe2 site is rhombically distorted with three short FeO bond distances of 1.950 ± 0.015 Å and three longer ones 2.053, 2.147, and 2.244 Å. The average bond lengths around the two iron atoms are significantly different as expected for a mixed-valent species with localized valences: those around Fe1 average 2.136 Å while those around Fe2 average 2.049 Å. The most important difference is found in the distances from the two iron atoms to the bridging phenolate oxygen: 1.949 Å (Fe2−O1) vs 2.073 Å (Fe1−O1). Similar differences in bond lengths are observed for complexes of the tetrapyridyl[14] (1.943 and 2.090 Å) and tetraimidazole[15] (1.958 and 2.115 Å) ligands. This clearly identifies Fe2 as the ferric site and Fe1 as the ferrous one. The ferrous site (Fe1) is analogous to those found in complexes of the tetrapyridyl and tetraimidazole ligands, and its metrical parameters match theirs. On the other hand, the ferric site (Fe2) could be expected to resemble those found in complexes involving mixed phenol-pyridin[19,20] and phenol-imidazole[21] branches. However the aminophenol group used here does not allow the oxygen of the terminal phenol to occupy the position trans to the bridging phenolate oxygen as in the latter complexes. This makes the ferric site of **1a** quite different with the two Fe−O(phenolate) bonds comparable in lengths (Fe2−O1: 1.949 Å and Fe2−O2: 1.936 Å), while they differ strongly in the above mentioned complexes[19−21] (ca. 1.86 and 2.09 Å, respectively, as an average). Therefore the ferric site of **1a** is more alike the ferric sites found in the tetrapyridyl and tetraimidazole ligands. Finally it is worth noting that the two carboxylate groups are bound asymmetrically to the diiron center: the two Fe−O bonds in the *trans* positions to the tertiary amines are significantly shorter than the two others (Fe1O4: 2.037 Å vs Fe1O6: 2.178 Å and Fe2O5: 1.965 Å vs Fe2O3: 2.053 Å).

Electronic Absorption Spectroscopy. Table 3 lists the absorption maxima and extinction coefficients for all complexes prepared in this work. As can be seen the spectra of the mixed-valent complexes are dominated in the visible range by a band in the 500−600 nm domain. In addition they exhibit a strong band at higher energy, $\lambda \sim 330-370$ nm, and a low intensity band at $\lambda \sim 1050$ nm. Figure 2 illustrates the electronic absorption spectrum of **1a** in acetonitrile. This spectrum presents four distinct features: two shoulders at 376 nm (ϵ = 2500 mol^{-1}·cm^{-1}) and 404 nm (ϵ = 2350 mol^{-1}·cm^{-1}), a band at 548 nm (ϵ = 1900 mol^{-1}·cm^{-1}), and an additional shoulder on the lower energy side of this band at 1050 nm (ϵ = 160 mol^{-1}·cm^{-1}). The $Fe^{II}Fe^{III}$ derivatives of the tetrapyridyl ligand[13,14] exhibit a band around 550 nm which has been assigned to a charge transfer (CT) from the bridging phenolate to the ferric ion, a transition at higher energy (λ ca. 330 nm) attributed to a charge transfer from the ferrous ion to the pyridyl groups and a band at lower energy (λ ca. 1200 nm) assigned to the intervalence (IV) transition. By analogy it seems reasonable to assign the various transitions of **1a** in the order of decreasing energy as the $Fe^{II} \rightarrow$ py CT, the terminal phenolate $\rightarrow Fe^{III}$ CT, the bridging phenolate $\rightarrow Fe^{III}$ CT, and the IV transition. Alternatively the latter transition could originate from a d−d transition of the ferrous ion; such transitions have been shown to appear in this domain in *semimet* hemerythrins.[30] However, the correlation observed in several derivatives between the energy of this band and the electrochemical potentials supports its assignment as the IV transition (see below). The respective assignments of the CT transitions of the two phenolates is supported by the observation that in the derivatives of H_2L2 only one band is detected in the 400−600 nm range but with an almost double intensity: in these compounds the two phenolates are more similar and the two CT bands are not distinguished. This CT transition is sensitive to the nature of the additional bridges (e.g., mpdp, benzoate, diphenylphosphate). It can be seen from Table 3 that the more electron donating these bridges, the higher the energy of the CT band: its variation as mpdp > benzoate > diphenylphosphate is in line with the known electronic properties of these groups. In the diferric complexes this CT transition occurs at lower energy: $\lambda \sim 630-$

(30) McCormick, J. M.; Reem, R. C.; Solomon, E. I. *J. Am. Chem. Soc.* **1991**, *113*, 9066.

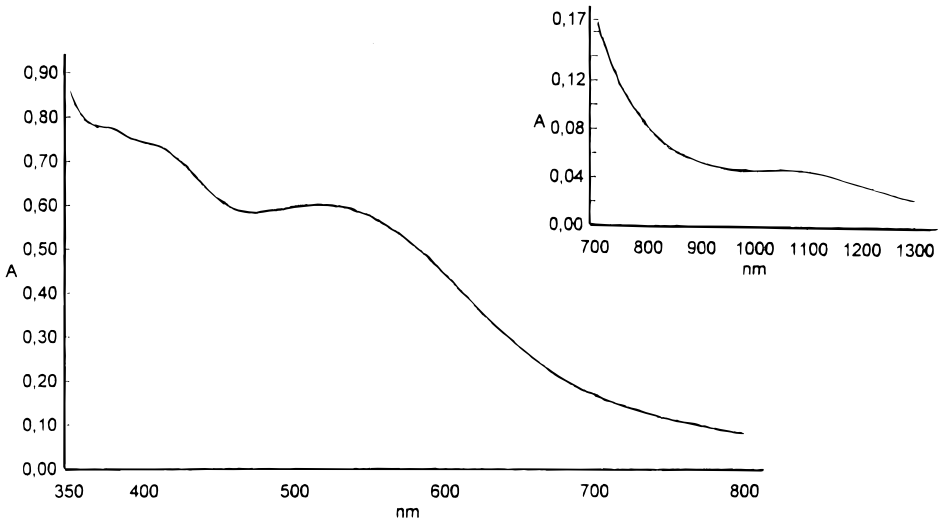

Figure 2. Electronic absorption spectrum of complex **1a** in acetonitrile.

Table 3. Maximum Wavelengths (nm) and Extinction Coefficient (mol^{-1} cm^{-1}) of Mixed-Valent and Diferric Complexes in Acetonitrile

mixed-valent/diferric compds	λmax (ϵ) $Fe^{II}Fe^{III}$	λmax (ϵ) $Fe^{III}Fe^{III}$
1a/3a	376 (2500); 404 (2350); 548 (1900); 1050 (160)	616 (1970)
1c	395 (300); 528 (2250); 1050 (160)	
1d/3d	370 (3020); 550 (1950); 1050 (100)	640 (1900)
1′a/3′a	400 (7800); 496 (3400); 1120 (230)	566
2c/4c	330 (5500); 562 (3250); 1050 (300)	630
2d/4d	360 (4000); 580 (3300); 1050 (90)	325 (5250); 360 (4150); 657 (3450)

660 nm. This shift is consistent with the energy of the Fe^{III} orbitals decreasing upon oxidation of the diiron center.

Resonance Raman Spectroscopy. The mixed-valent complexes **1a** and **2d** were studied by resonance Raman spectroscopy at several excitation wavelengths in the 400−700 nm range. Owing to strong photoreduction, it was not possible to get reliable results for the diferric complex **3c**. **1a** and **2d** show a set of four Raman bands in the 1150−1600 cm^{-1} range whose frequencies are associated with phenolate ring vibrations and a band at ca. 620 cm^{-1} that is usually assigned to a vibration with Fe−O character.[31] The main difference between the two complexes is that all the bands are split into doublets (even a closely spaced triplet for the 1296 cm^{-1} band) in the case of **2d**, whereas only weak shoulders are present on the main bands in the case of **1a** (Figure 3). The excitation profiles of these bands were established; they reveal a maximum at a wavelength close to the maximum of the visible absorption band (in fact slightly red-shifted by ca. 1000−2000 cm^{-1}). For complex **1a** the enhancement factors are modest, while for **2d** a marked resonant effect is observed for the main Raman bands. This is in agreement with the higher visible extinction coefficient of the latter.

These results bring support for the assignment of the visible absorption band to the phenolate → Fe(III) CT transition. The resonance Raman spectrum of **2d** is strikingly analogous to the spectra of the ferric complexes of *ortho* substituted phenolates.[31b,c] Indeed, they display characteristic splittings of the main Raman bands that originate in the lower symmetry of the *ortho* relative to *para* substituted phenolates. Complexes **1a** and **2d** contain two different ortho substituted phenolates: a terminal one and a bridging one; the latter is bis-ortho substituted and displays C_{2v} symmetry, while the former retains the low symmetry of

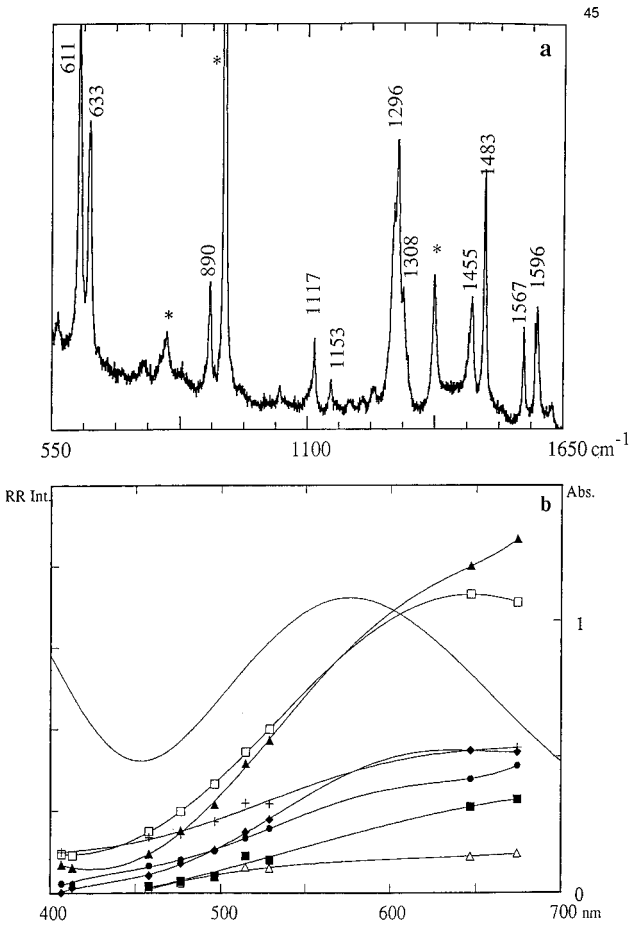

Figure 3. (a) Resonance Raman spectrum of complex **2d** in acetonitrile, obtained by excitation at 647.1 nm, *: solvent band; (b) excitation profile of the main Raman bands: ◆, 1595 cm^{-1}; ●, 1565 cm^{-1}; □, 1482 cm^{-1}; +, 1455 cm^{-1}; ▲, 1295 cm^{-1}; △, 1153 cm^{-1}; ■, 1115 cm^{-1}.

(31) (a) Que, L. In *Biological Applications of Raman Spectroscopy*; Spiro, T. G., Ed.; Wiley: New York, 1988; Vol. 3, pp 491−521. (b) Gaber, B. P. Miskowski, V.; Spiro, T. G. *J. Am. Chem. Soc.* **1974**, *96*, 6868. (c) Carrano, C. J.; Carrano, M. W.; Sharma, K.; Backes, G.; Sanders-Loehr, J. *Inorg. Chem.* **1990**, *29*, 1865.

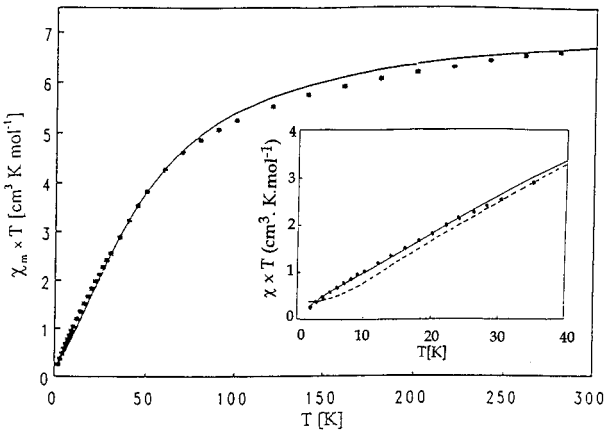

Figure 4. Temperature dependence of the product of molar susceptibility (χ) by temperature for complex **1a**. Insert: low temperature (2−40 K) data; dotted line: best fit with Heisenberg exchange Hamiltonian; solid line: best fit with eq 1 (see text).

ortho substituted phenolates. Therefore the spectrum of **2d** is assigned to the terminal phenolate. Complex **1a** differs from complex **2d** mainly by the size of the chelate ring on the Fe(III) atom: for **1a** a pseudo 2-fold symmetry is restored by the five-membered chelate ring, while for **2d** the six-membered ring is highly asymmetric; this may explain why only minor splittings of the phenolate Raman bands are observed in this case.

Magnetic Susceptibility Studies. Figure 4 illustrates for **1a** the temperature dependence of the product of the molar susceptibility (χ) by temperature. χ·T decreases smoothly from 6.8 K·cm^3·mol^{-1} at 300 K to 5.4 K·cm^3·mol^{-1} at 100 K and then more abruptly to reach 0.4 cm^3·mol^{-1} at 2 K. This behavior is characteristic of a $Fe^{II}Fe^{III}$ pair exhibiting a weak antiferromagnetic coupling between the two high spin ions and a moderate zero-field splitting of the ferrous ion. These data were fitted with the equation deduced from a Heisenberg Hamiltonian ($\boldsymbol{H} = -2J\,\mathbf{S_1}\cdot\mathbf{S_2}$) for two spins $S_1 = 5/2$ and $S_2 = 2$. The best fit was obtained for $g = 2.0$ and $J = -3.8$ cm^{-1}. Slightly higher values of J were obtained for the $Fe^{II}Fe^{III}$ acetate and diphenylphosphate derivatives of H_2L1 (**1b**: −4.9 cm^{-1}; **1d**: −5.2 cm^{-1}) and the $Fe^{II}Fe^{III}$ and $Fe^{III}Fe^{III}$ diphenylphosphate complexes of H_2L2 (**2d**: −4.5 cm^{-1}; **4d**: −6.8 cm^{-1}). These exchange couplings are close to the ones evaluated for the diiron derivatives of the symmetrical phenol dinucleating ligands (J in the range −1.5 to −6 cm^{-1}).[13−23]

With such a weak exchange coupling the use of Heisenberg Hamiltonian for mixed-valent $Fe^{II}Fe^{III}$ is not perfectly valid. Therefore a more complete analysis was performed using data collected at six magnetic fields in the range 0.5−5 Teslas over the 2−300 K temperature range. Experimental data were simulated with the following Hamiltonian which takes into account both the exchange interaction and the anisotropy of the individual ions:

$$\boldsymbol{H} = -2J\,\mathbf{S}_1\cdot\mathbf{S}_2 + \sum_i [D_i(S_{iz}^{\,2} - 2) + E_i(S_{ix}^{\,2} - S_{iy}^{\,2}) + \boldsymbol{H}_i]$$

$$\boldsymbol{H}_i = \beta(g_x H_x S_{ix} + g_y H_y S_{iy} + g_z H_z S_{iz}) \quad i = 1, 2$$

J is the isotropic exchange integral, D_i and E_i are the axial and rhombic zero-field splitting parameters respectively, and g_{ik} ($k = x, y, z$) are the components of the g tensors of the uncoupled ions. The usual assumption is made that the zero-field splitting and g tensors can be diagonalized simultaneously. Fitting of the data was realized under the assumption that the ferric site is isotropic: $g_1 = 2.0$, $D_1 = E_1 = 0$ and that the rhombicity of the ferrous site is negligeable $E_2 = 0$ (this was checked by independent calculations). The best fit (Figure 4) was obtained with the following parameters $J = -4.0(2)$ cm^{-1}, $g_2 = 2.09$, and $D_2 = -13(1)$ cm^{-1}. These results confirm that the exchange interaction and the zero-field splitting of the ferrous ion are of the same order of magnitude.

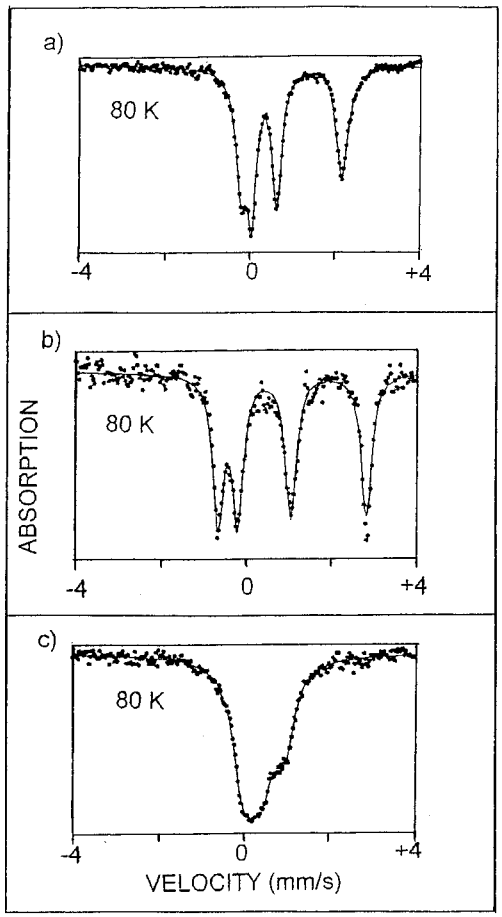

Figure 5. Mössbauer spectra of compounds **1a** (a), **2d** (b), and **4d** (c).

Mössbauer Spectroscopy. The Mössbauer spectra of complexes **1a**, **2d**, and **4d** recorded at 292 and 80 K consist of two quadrupole split doublets with equivalent absorption areas, as shown in Figure 5 for the 80 K spectra. They were least-squares fitted with Lorentzian lines, and the resulting isomer shift (δ) and quadrupole splitting parameters (ΔE_Q) are listed in Table 4. The $\delta = 0.490$ and $\Delta E_Q = 0.594$ mm·s^{-1} values and the minute thermal variation of ΔE_Q in the 80−293 K range (0.594−0.547 mm·s^{-1}) clearly indicate the presence of a high-spin iron (III) site in **1a**, while the $\delta = 1.124$ and $\Delta E_Q = 2.376$ mm·s^{-1} values of the second doublet are typical of a high-spin ferrous site.[32] The half-width of the absorptions ($\Gamma/2$) is in the usual range and does not show any significant temperature dependence, indicating that the iron valences are localized in the solid state for this $Fe^{II}Fe^{III}$ complex. A similar behavior has been described for related compounds[13,14,16] although in some cases partial valence delocalization has been observed in the high-temperature range.[15,33]

The Mössbauer spectrum of **2d** (Figure 5b) is similar to that of **1a**, the main difference being the larger quadrupole splittings of both the ferrous and ferric sites. The large 80 K ΔE_Q (Fe(II)) value indicates that the T_{2g} orbital triplet is split by crystal

(32) Greenwood, N. N., Gibbs, T. C., *Mössbauer Spectroscopy*; Chapman and Hall: New York, 1971.

(33) Maeda, Y.; Tanigawa, Y.; Matsumoto, N.; Oshio, H.; Suzuki, M.; Takashima, Y. *Bull. Chem. Soc. Jpn.* **1994**, *67*, 125.

Table 4. Mössbauer Data of Complexes **1a**, **2d**, and **4d**[a,b]

compd	N_3O_3 site (Fe^{II} or Fe^{III})			N_2O_4 site (Fe^{II} or Fe^{III})			
	δ	ΔE_Q	$\Gamma/2$	δ	ΔE_Q	$\Gamma/2$	T (K)
1a	1.124(2)	2.376(4)	0.158(3)	0.490(2)	0.594(3)	0.133(2)	80
	0.979(4)	1.807(7)	0.137(5)	0.414(3)	0.547(5)	0.125(3)	293
(2d)	1.183(4)	3.358(7)	0.148(4)	0.550(4)	1.220(7)	0.148(4)	80
	1.078(7)	2.74(2)	0.15(1)	0.448(6)	1.21(1)	0.14(1)	293
(4d)	0.447(5)	0.31(2)	0.276(8)	0.570(5)	0.99(2)	0.276(8)	80
	0.343(6)	0.29(3)	0.34(2)	0.47(1)	1.06(4)	0.34(2)	293
$[Fe^{III}Fe^{III}$(LPy3Bn)(mpdp)$](BPh_4)$[27]	0.475(4)	0.329(6)	0.198(6)	1.196(4)	2.657(7)	0.217(7)	80
	0.336(3)	0.364(6)	0.101(9)	1.176(8)	1.75(2)	0.15(1)	293

[a] δ = isomer shift (mms^{-1}). ΔE_Q = quadrupole splitting (mms^{-1}). $\Gamma/2$ = half-width of the lines. [b] Statistical standard deviations are given in parentheses.

field distortions affording lower than octahedral symmetry and that the lower state is an orbital singlet. The moderate 80−293 K ΔE_Q thermal variation (Table 4) suggests a partial thermal population of the higher orbital states at 293 K indicating that the energy separation between the singlet ground state and the higher orbital states is larger than kT[34] (a rough evaluation affords ∼650 cm^{-1}). Both observations point out to a significant axial distortion of the iron(II) cubic ligand field. A similar qualitative analysis can be made for the ferric site of **2d**, and it may be suggested that the larger axial distortion of the cubic ligand field of both iron sites in **2d** compared to **1a** results either from structural constraints imposed by the H_2L_2 ligand and/or the phosphate bridge or differences in the electronic structure of the donor atoms. Similarly to **1a**, the half-width of the absorptions ($\Gamma/2$) is in the usual range and does not show any significant temperature dependence, indicating that the iron valences are also localized in the solide state for **2d**. The asymmetric polydentate H_2L1 and H_2L2 ligands associated with the mpdp dicarboxylate (**1a**) and diphenyl phosphate (**2d**) bridges affording similar N_3O_3 and N_2O_4 donor sets to the iron centers of **1a** and **2d**: a similar valence localization is expected for both complexes with Fe(II) located at the N_3O_3 site and Fe(III) at the N_2O_4 one.

Figure 5c shows the 80 K Mössbauer spectrum of the bis-ferric diphenylphosphate derivative **4d** in which, as expected, the isomer shifts of both sites (a and b) are in the 0.4−0.6 $mm{\cdot}s^{-1}$ range. However, the quadrupole splitting of site a (δ = 0.570, ΔE_Q = 0.988 $mm{\cdot}s^{-1}$) is much larger than that of site b (δ = 0.447, ΔE_Q = 0.305 $mm{\cdot}s^{-1}$) pointing out to quite different local symmetries for the ferric sites a and b of **4d**. Assignation of sites a and b can be made on the following grounds: (i) site a is characterized by quadrupole splitting and isomer shift values close to those of the N_2O_4 site of **2d** (δ = 0.550, ΔE_Q = 1.220 $mm{\cdot}s^{-1}$), (ii) the isomer shift of site a is 0.12 $mm{\cdot}s^{-1}$ larger than that of site b, in agreement with the larger electron density induced onto the iron by a N_2O_4 compared to a N_3O_3 donor set, and (iii) site b is characterized by quadrupole splitting and isomer shift values close to those of the N_3O_3 ferric site of the mixed-valence derivative of the benzyl ligand[27] (δ = 0.475, ΔE_Q = 0.329 $mm{\cdot}s^{-1}$, Table 4).

NMR Spectroscopy. As seen in Figure 6, the NMR spectra of **1a** and **2d** extend over a very wide frequency range of ca. 600 ppm, from 540 to −50 ppm for **1a** and from 560 to −100 ppm for **3d**. This behavior differs significantly from the one exhibited by the mixed-valent complexes of the tetrapyridyl[14] and tetraimidazolyl[15] ligands whose spectral range covers only 400 ppm and is restricted to positive chemical shifts. In the latter complexes the number of peaks is reduced by the 2-fold symmetry showing that the valences of the two iron atoms are delocalized on the NMR time scale. It is worth noting that, in this series of compounds, negative chemical shifts are associated to methylenic protons close to a ferrous center.[35] Therefore, both the extended spectral range and the presence of signal at negative chemical shifts strongly suggest that **1a** and **2d** are valence localized at room temperature. This has been confirmed by variable temperature NMR experiments.[27]

Table SM2 (Supporting Information) lists the assignments of the signals and scheme SM1 depicts the proton labeling. The signals have been assigned through chemical substitution and a combination of NMR techniques involving T_1 measurements and 1D NOE and 2D COSY experiments as well as variable temperature experiments. In addition, the thorough studies of the homo-[35a,b] and heteronuclear[35c] $Fe^{II}M^{II}$ derivatives of the tetrapyridyl ligand were used to validate the assignments. Extensive NMR studies of the latter compounds have shown that methylenic and *ortho*-pyridyl protons close to a ferrous ion have signals confined to a narrow range whatever the nature of the second metal (M^{II} = Zn^{II}, Co^{II}, Fe^{II}, Mn^{II}). The two protons of each methylene group are structurally constrained by the formation of the metallacycles and therefore related to each other as are axial and equatorial cyclohexane protons. As a consequence their isotropic shifts are rather strictly correlated which helps assign them unambiguously.[35b,36] Accordingly taking into account both the value of the spin and the value of the dihedral angle of the protons with respect to the metallacycle leads to the assignment summarized in Table SM2. The magnitude COSY spectrum of **1a** recorded in the 250 ppm spectral range reveals several correlations between aromatic protons. The first one involves signals at −51, 70, −33, and 50 ppm. The alternating signs of the chemical shift indicate that the corresponding protons belong to an aromatic ring, in this case the terminal phenolate. However, a doubt remains about the two following possible assignments: Pho-Phm-Php-Phm′ and Phm′-Php-Phm-Pho. This uncertainty has been resolved by a NOE experiment which showed a correlation between the peak at −33 ppm and the one at 90 ppm assigned to the axial methylenic proton of the third picolyl group and another correlation between the peak at 70 ppm and the one at 206 ppm assigned to the *o*-pyridyl proton of the third picolyl group. Correlations exist also between the *meta*, *para*, and *meta*′ protons of two pyridyl groups in the sequences 59 ↔ 10 ↔ 35 ppm and 75 ↔ 5 ↔ 85 ppm. The former corresponds to a pyridyl bound to Fe^{II}, while the latter is associated to the pyridyl bound to Fe^{III}. Owing to their very short T_1 the *o*-pyridyl protons cannot be observed in the 2D experiments. The protons of the second pyridyl of the bis-picolylamine branch have not been assigned specifically.

(34) Sams, J. R.; Tsin, T. B. *Inorg. Chem.* **1975**, 14, 1573 and references therein.

(35) (a) Borovik, A. S.; Hendrich, M. P.; Holman, T. R.; Münck, E.; Papaefthymiou, V.; Que, L., Jr. *J. Am. Chem. Soc.* **1990**, *112*, 6031. (b) Ming, L. J.; Jang, H. G.; Que, L., Jr. *Inorg. Chem.* **1992**, *31*, 359. (c) Wang, Z.; Holman, T. R.; Que, L., Jr. *Magn. Reson. Chem.* **1993**, *31*, S78.

(36) Holm, R. H.; Hawkins, C. J. In *NMR of Paramagnetic Molecules, Principles and Applications*; LaMar, G. N., Horrocks, W. DeW., Jr., Holm, R. H., Eds.; Academic Press: New York, 1973.

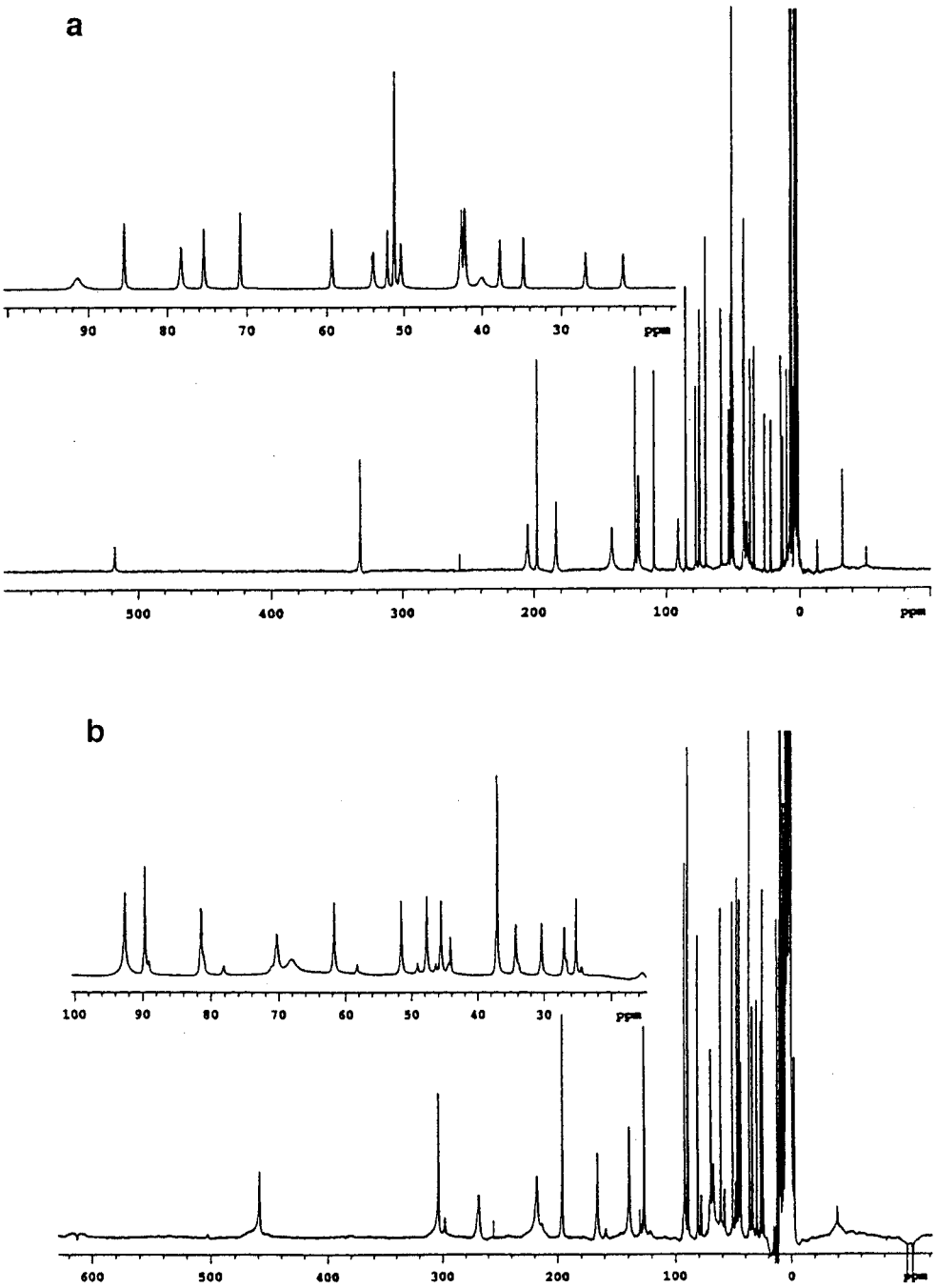

Figure 6. NMR spectra of compounds **1a** and **2d** in CD_3CN.

Their signals overlap with those of the mpdp ligand, and they have been observed independently only at low temperature (ca. 220 K). The dicarboxylate protons were identified by chemical substitution and assigned from COSY experiments. The high isotropic shift (δ = 110 ppm) of the *ortho* proton is worth noting. Actually the resonances of the corresponding *meta* protons appear at 42 ppm only in spite of the fact that both the *ortho* and *meta* protons are linked to the Fe ions through the same number of bonds and should therefore have similar delocalized spin densities. The chemical shift difference points to a strong dipolar contribution to the isotropic shift of the *ortho* proton in line with its short distance to both Fe ions.

As shown in Figure 6b the spectrum of **2d** differs from the one of **1a** in the lack of the mpdp resonances in the 20−40 ppm domain, those of the phenyl groups of dpp being in the 0−10 ppm range. Besides one additional signal is observed at 461 ppm which corresponds to the equatorial proton of the methylene group linked to the terminal phenol. COSY experiments have identified the protons of this phenol with their expected alternating positions, and the *meta*, *para*, and *meta′* protons of the three pyridyls (see Table SM2).

Electrochemistry. The electrochemical properties of the various complexes have been investigated in acetonitrile solution with tetrabutylammonium perchlorate as supporting electrolyte. The potentials were referenced toward Ag/10 mM Ag^+ electrode. Cyclic voltammograms of a solution of **1a** are depicted in Figure 7. On the oxidation side (curve a) it comprises one reversible couple at a half-wave potential of $E_{1/2}(\text{ox}) = 0.11$ V ($E_{p_a} = 0.14$ V, $E_{p_c} = 0.07$ V, $\Delta E_p = 70$ mV). Exhaustive electrolysis of the solution at a potential of 0.35 V requires one Faraday per mol. When this solution is electrolyzed again at a potential of 0 V, the starting solution is regenerated after consumption of one Faraday·mol^{-1} as judged from voltamperometry and visible spectroscopy. These results show that the electrochemical process involved is the reversible one-electron oxidation of the mixed-valent $Fe^{II}Fe^{III}$ complex into its diferric

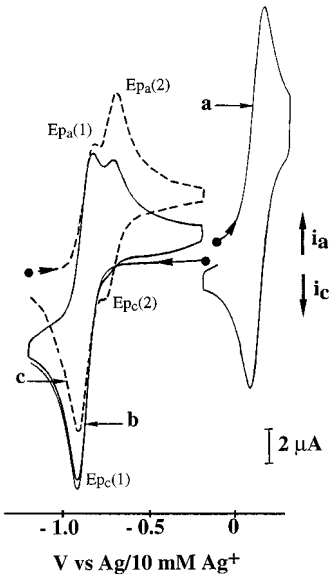

Figure 7. Cyclic voltammograms on glassy carbon electrode (diameter 3 mm) of a solution of **1a** 0.8 mM in acetonitrile containing 0.1 M TBAP; $\upsilon = 100$ mV·s^{-1}. Curve a: scan in the range −0.10 to +0.30 V; curve b: scan in the range −0.15 to −1.20 V; curve c: obtained after controlled electrolysis of the initial solution at −1.20 V.

$Fe^{III}Fe^{III}$ counterpart. The reduction behavior is more complicated. Actually, during the first reduction-reoxidation cycle (curve b), the cyclic voltammogram exhibits one reduction peak at $E_{p_c}(1) = -0.91$ V and two reoxidation peaks at $E_{p_a}(1) = -0.83$ V and $E_{p_a}(2) = -0.68$ V. Exhaustive electrolysis of the solution at a potential of −1.20 V requires one Faraday per mol. The cyclic voltammogram of the resulting solution is illustrated in Figure 7 curve c. It is constituted by two oxidation peaks at $E_{p_a}(1) = -0.83$ V and $E_{p_a}(2) = -0.68$ V and two reduction peaks at $E_{p_c}(1) = -0.91$ V and $E_{p_c}(2) = -0.77$ V. Therefore reduction of **1a** gives rise to two distinct $Fe^{II}Fe^{II}$ species with half-wave potentials of $E_{1/2}(\text{red1}) = -0.87$ V and $E_{1/2}(\text{red2}) = -0.74$ V. The two redox couples correspond to reversible one-electron transfers. Comparison of wave heights of the voltamperogram shows that the ratio of the two species is close to 50:50. When the reduced solution is reoxidized at a potential of −0.40 V, the initial solution is regenerated after consumption of one Faraday per mol. Moreover when the reduced solution is reoxidized at −0.80 V, a potential located in between $E_{1/2}$(red1) and $E_{1/2}$(red2), the final solution contains approximately 50% of **1a** and 50% of a 50:50 mixture of the two $Fe^{II}Fe^{II}$ species. These results show that the species formed at $E_{p_c}(1) = -0.91$ V is the one-electron reduced counterpart of **1a** and that the two reduced species are in chemical equilibrium.

The occurrence of the chemical equilibrium between the two $Fe^{II}Fe^{II}$ species is further supported by cyclic voltammetry experiments. Actually the height of the second reoxidation peak ($E_{p_a}(2) = -0.68$ V) depends on the potential scan rate in the range 10−1000 mV/s and maximizes at ca. 50 mV/s. This finding indicates that the rate of formation of this species from reduced **1a** through the equilibrium is of the same order of magnitude as the reoxidation of reduced **1a**; thus on the time scale of the cyclic voltammetry the system has not reached equilibrium what it does in the exhaustive electrolysis experiment.

In order to get more information on the electronic factors of importance for these redox reactions and on the nature of the second reduced species, two other complexes similar to **1a** were synthesized and their electrochemical properties investigated. In complex **1c** the bridging *m*-phenylenedipropionate was substituted by the less electron-donating benzoate. Complex

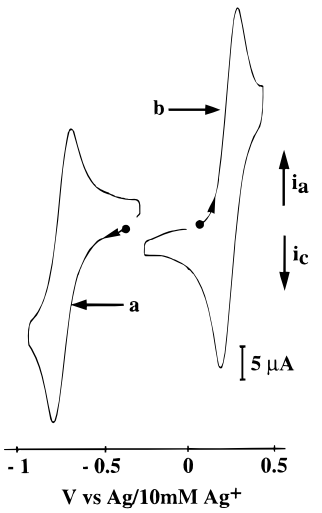

Figure 8. Cyclic voltammogram on a Pt electrode (diameter 5 mm) of a solution of **1d** 1.0 mM in acetonitrile containing 0.1 M TBAP; v = 100 mV·s^{-1}. Curve a: scan in the range −0.40 to −0.95 V; curve b: scan in the range −0.30 to +0.40 V.

1c exhibits the same electrochemical behavior as **1a** with, as expected, a shift in the half-wave potentials toward more positive values: a similar 30 mV shift is observed both for the oxidation and for the reduction of the mixed-valent complex. Interestingly, after reductive electrolysis the ratio of the two $Fe^{II}Fe^{II}$ derivatives was not equal anymore and amounted to ca. 60:40 indicating that in this case the chemical equilibrium is less displaced toward the second species.

Complex **1′a** was synthesized as **1a** from the *p*-nitrophenolate ligand $H_2L'1$ (Scheme 1, R = NO_2). This ligand was designed for introducing a strongly electron-withdrawing group onto the terminal phenolate so as to alter significantly the electrochemical behavior of the complex. As for **1a** a reversible one-electron transfer is present in the oxidation domain which corresponds to the $Fe^{II}Fe^{III}/Fe^{III}Fe^{III}$ couple. This oxidation occurs at $E_{1/2}(\text{ox}) = 0.18$ V, a potential 70 mV higher than the corresponding one for **1a**. This shift is quite consistent with the electron-withdrawing influence of the nitro group which disfavors the oxidized form of the complex. On the reductive side the formation of two species is observed again as for **1a** and **1c**. The half-wave potentials of the two reversible processes are −0.69 and −0.57 V, ca. 180 mV less negative than the corresponding potentials for **1a**. As in the case of the benzoate, the ratio of the two Fe^{II} Fe^{II} derivatives is close to 60:40 pointing to a less displaced equilibrium with respect to **1a**. Also of interest is the fact that the rate of formation of the second reduced species is notably slower than for **1a** as judged from the sweep rate dependency of the cyclic voltammograms.

Figure 8 illustrates cyclic voltammograms of the bis-diphenylphosphate complex $[Fe_2(L1)(dpp)_2](PF_6)$, **1d**. The electrochemical behavior of this compound departs from the one of the carboxylate derivatives since it is reduced in a single reversible one-electron transfer at $E_{1/2}(\text{red}) = -0.75$ V (curve a: $E_{p_a} = -0.72$ V, $E_{p_c} = -0.78$ V, $\Delta E_p = 60$ mV) pointing to the formation of a single reduced species. Similarly it is oxidized in a reversible one-electron transfer at $E_{1/2}(\text{ox}) = 0.21$ V (curve b: $E_{p_a} = 0.24$ V, $E_{p_c} = 0.17$ V, $\Delta E_p = 70$ mV). The values of the potentials are higher than those of **1a** and **1c** in agreement with the fact that the diphenylphosphate is less electron donating than the carboxylates.

The complexes of ligand H_2L2 exhibit the same behavior as **1d**. The oxidation occurs at $E_{1/2}(\text{ox}) = 0.07$ and 0.16 V, respectively, for **2c** and **2d**, and the reduction at $E_{1/2}$ (red) =

Table 5. Electrochemical Data of Mixed-Valent Diiron Derivatives[a] of Phenolato Ligands in Acetonitrile ($E_{1/2} = (E_{p_a} + E_{p_c})/2$; See Text)

compd	$E_{1/2}$ (ox) (V_{NHE})	$E_{1/2}$ (red 2) (V_{NHE})	$E_{1/2}$ (red 1) (V_{NHE})	ΔE (V)	K_{com}	ref
1a	0.63	−0.22	−0.35	0.98	3.8×10^{16}	b
1c	0.66	−0.23	−0.32	0.98	3.8×10^{16}	b
1d	0.73		−0.23	0.96	1.7×10^{16}	b
1′a	0.70	−0.05	−0.17	0.87	5.2×10^{14}	b
2b	0.62		−0.25	0.87	5.2×10^{14}	23
2c	0.59		−0.28	0.87	5.2×10^{14}	b
2d	0.68		−0.23	0.91	2.5×10^{15}	b
$[Fe^{II}Fe^{III}(LPy_3Bn)(mpdp)](BPh_4)$	1.03		0.17	0.82	7.4×10^{13}	27
$[Fe^{II}Fe^{III}(LPy_4)(dpp)](ClO_4)_2$	1.00		0.38	0.62	3.1×10^{10}	17
$[Fe^{II}Fe^{III}(LPy_4)(mpdp)](ClO_4)_2$	0.88		0.15	0.73	2.2×10^{12}	c
$[Fe^{II}Fe^{III}(LBzIm_4)(OAc)_2](BF_4)_2$	0.80		0.12	0.68	5×10^{11}	16
$[Fe^{II}Fe^{III}(LIm_4)(OAc)_2](ClO_4)_2$	0.68		0.02	0.66	3×10^{11}	15
$[Fe^{III}Fe^{III}(LIm_2PhO_2)(OAc)_2](ClO_4)$	−0.03		−0.59	0.56	4×10^{9}	21
$[Fe^{III}Fe^{III}(LPy_2PhO_2)(OAc)_2](ClO_4)$	−0.38		−0.96	0.58	6.5×10^{9}	19

[a] For the tetraphenylborate salts the irreversible oxidation of the anion ($BPh_4^- \rightarrow BPh_3$) occurred at $E_{p_a} = 0.6$ V_{NHE}; literature potentials were converted to the normal hydrogen electrode according to Bard, A. J.; Faulkner, L. R. *Electrochemical Methods. Fundamentals and Applications*; Wiley: New York, 1980. [b] This work. [c] Maeda, Y.; Tanigawa, Y.; Hayami, S.; Takashima, Y. *Chem. Lett.* **1992**, 591.

−0.80 and −0.75 V. The values of these potentials are in agreement with the lower donating ability of diphenylphosphate with respect to benzoate.

Discussion

Stability of the Mixed-Valent Species. Examination of Table 5 shows that the potential difference between the oxidation and the first reduction of the mixed-valent species is strongly dependent upon the organic ligand used and less so on the bridging carboxylate/phosphate anion. The complexes of H_2-L1 exhibit $\Delta E_{1/2} = E_{1/2}$(ox) - $E_{1/2}$(red or red1) of 975 ± 5 mV and those of H_2L2 $\Delta E_{1/2} = 890 \pm 10$ mV. This increased stability domain of the mixed-valent form in the present system can be quantitated through the equilibrium constant K_{com} of the comproportionation reaction

$$[Fe^{II}Fe^{II}(L)(X)_2] + [Fe^{III}Fe^{III}(L)(X)_2]^{2+} \Leftrightarrow 2[Fe^{II}Fe^{III}(L)(X)_2]^{+}$$

where $(X)_2$ = mpdp, $(OBz)_2$, or $(dpp)_2$ and $H_2L = H_2L1$ or H_2L2. The potential difference is related to the comproportionation constant by the equation

$$\Delta E = (RT/nF) \ln K_{com}$$

This relationship establishes that the larger the potential difference the more stable the mixed-valent species. The use of this relation leads to estimate K_{com} at ca. $1-4 \times 10^{16}$ for complexes of H_2L1 and $0.5-3 \times 10^{15}$ for complexes of H_2L2. ΔE and K_{com} values of the mixed-valent complexes of the tetrapyridyl and dipyridyldiphenol ligands are listed in Table 5. These symmetrical compounds exhibit quite different behaviors since ΔE values are 300−400 mV smaller and K_{com} values 2 to 4 orders of magnitude lower than those of the present unsymmetrical compounds.

Gagné *et al.*[37] have identified the various factors influencing the stability of the mixed-valent forms of dinuclear metal compounds. These are (i) structural changes associated to the redox reactions; (ii) coulombic interactions; (iii) magnetic exchange between the metal centers; (iv) electronic delocalization which is expected to stabilize the mixed-valent form. Que *et al.*[14] have discussed the importance of the latter effects in complexes of the tetrapyridyl ligand through comparison of the $Fe^{II}Fe^{III}$ complex with the heterobinuclear $Fe^{II}Ga^{III}$ and Zn^{II}-Fe^{III} derivatives. Their conclusion was that electronic delocalization plays a moderate role bringing an estimated stabilization of ca. 100 mV of the II,III state toward oxidation. However NMR studies[27] have shown that the present complexes are valence localized in solution at room temperature, while those of the tetranitrogen ligands are delocalized. Therefore, this factor cannot explain the higher stabilization observed for the $Fe^{II}Fe^{III}$ derivatives of H_2L1 and H_2L2.

If different magnetic exchange interactions were operative in the different redox forms, they would afford different stabilizations. However magnetic susceptibility studies using the Heisenberg hamiltonian ($\boldsymbol{H} = -2J\mathbf{S}_1\cdot\mathbf{S}_2$) allow to estimate the exchange interactions between the two iron atoms to ca. 5 K in the $Fe^{II}Fe^{III}$ complexes and ca. 10 K in the diferric compounds in agreement with the values observed in HLPy4[13,14] and HLIm4[15] derivatives. In the corresponding diferrous derivatives the exchange interaction is even weaker.[35a,38] As a consequence it is quite unlikely that magnetic exchange interactions play an important role in stabilizing any of the three species involved in the comproportionation equilibrium.

Coulombic interactions are expected not to differ significantly for complexes of the same ligand. However they may be of considerable importance when comparing derivatives of the tetrapyridyl ligand with those of the tripyridylphenolate and dipyridyldiphenolate ligands. From the data listed in Table 5, if the redox potential differences were linearly related to the ligand charges a ΔE close to 650 mV would be expected for diiron complexes of the tripyridyl ligands, at variance with the experimental results. In fact the situation is more complex since in the present derivatives the two sites are not equivalent and the ligand charges are not equally distributed. As a consequence the N_3O_3 site is more alike the HLPy4 sites and the N_2O_4 site closer to those of $H_3LPy_2PhO_2$. This peculiarity is clearly noted upon comparing the respective oxidation and reduction potentials of the various species. Indeed it reveals that the present mixed-valent complexes have oxidation potentials intermediate between those of the corresponding HLPy4 and $H_3LPy_2PhO_2$ derivatives while in reduction they behave more alike the latter. This behavior which results from the asymmetry of the ligands is the origin of the increased stability of the $Fe^{II}Fe^{III}$ state in the present complexes.

Complexes of the H_2L1 have a ΔE 100 mV larger than those of H_2L2. Since coulombic factors are conserved in the two series, their structural difference must be the cause of their

(37) Gagné, R. R.; Spiro, C. L.; Smith, T. J.; Hamann, C. A.; Thies, W. R.; Shiemke, A. K. *J. Am. Chem. Soc.* **1981**, *103*, 4073.

(38) Jang, H. G.; Hendrich, M. P.; Que, L., Jr. *Inorg. Chem.* **1993**, *32*, 911.

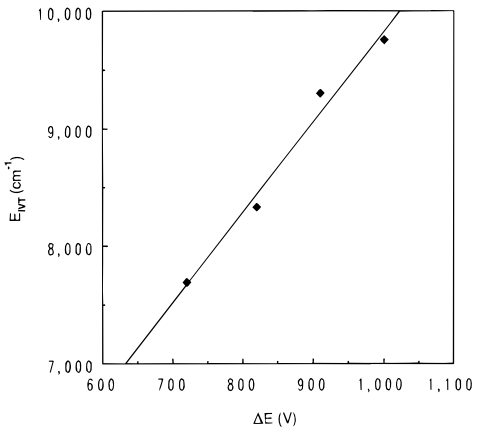

Figure 9. Correlation between the energy of the intervalence transition (E_{IVT}) and the stability domain (ΔE) of mixed-valent complexes.

different behavior. This structural difference most probably arises from the different sizes of the chelates in which the terminal phenolate is engaged: for complexes of H_2L1 the aminophenol group forms a five-membered ring with the iron while for those of H_2L2 a six-membered ring results from the presence of the extra methylene group. The change in electronic structure of the diiron center brought about by this structural effect is also clearly reflected in the quite different quadrupole splittings of the ferric site of **1a** and **2d** (see Table 4). It is well documented that the chelate ring size influences the redox potentials.

To summarize the above discussion the enhanced stabilization of the mixed-valent state in the present complexes can be attributed to the asymmetry in the coulombic interactions introduced by the ligands: it can be estimated to ca. 400 mV, if 100 mV due to the lack of stabilization through electronic delocalization in the symmetrical compounds are taken into account. This major effect is modulated by the specific structural influence of the binucleating ligand. Comparison of the potential difference with the energy of the intervalence transition of the mixed-valent complexes further supports the prominent role of the ligand asymmetry. It is well known that in asymmetrical compounds the difference in energy between the two sites adds to the energy associated to the electron transfer. Indeed, a good corrrelation is observed between ΔE and the energy of the IV transition as shown in Figure 9.

Potential of the $Fe^{II}Fe^{III}/Fe^{III}Fe^{III}$ Couple. Examination of Table 5 shows that the electrochemical potentials in acetonitrile of the various μ-phenoxodiiron complexes depend strongly on the number of terminal phenolates: substituting one pyridyl ligand by a phenolate lowers the potential of the $Fe^{II}Fe^{III}/Fe^{III}$-Fe^{III} couple by more than 200 mV. Therefore it is the number of terminal phenolates which tunes the oxidation potential of the $Fe^{II}Fe^{III}$ state. Conversely the nature of the bridging carboxylate/phosphate is less important. A thorough electrochemical study of uteroferrin[39] has shown that at pH 7 the mixed-valent form oxidizes at 240 mV. This value is respectively 200 and 300 mV higher than the reduction potential of the diiron site in RNR[40] and MMO[41] hydroxylase. This observation is at variance with the present study which stresses the stabilization of the diferric form by a terminal phenolate. In the proteins the individual influences of the various ligands can be opposed by medium effects.

Mechanism of Reduction of 1a−c. The carboxylate complexes of H_2L1 differ from the diphenylphosphate derivative **1d** and from all complexes of H_2L2 in that the diferrous compound obtained from the one-electron reduction of the mixed-valent complex is not stable and is in chemical equilibrium with another diferrous species. The electrochemical experiments can be summarized by the following equation

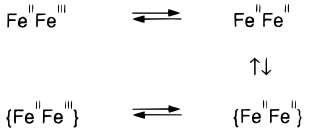

In all carboxylate complexes of H_2L1 the second reduced species exhibits oxidation potentials ca. 100−200 mV less negative than those of the first one (Table 5). This indicates that the decrease in electron density is the driving force of the transformation. This is further substantiated by the observation that the ratio of the two $Fe^{II}Fe^{II}$ species in equilibrium depends on the electron-donating ability of the ligands: while this ratio is close to 50:50 for **1a**, it approaches 60:40 (ie the equilibrium is less displaced toward the second reduced species) when the carboxylate (**1c**) or the ligand (**1′a**) are less electron donating. The overall chemical reversibility of the reduction−oxidation cycle argues against the occurrence of any drastic chemical change. It is then quite reasonable to think that the diferrous system lowers its high electron density through some simple chemical process which can be reversed through oxidation of the diiron center. Dissociation of an anionic ligand seems to be the easiest and most efficient and therefore the most likely process to achieve this withdrawal of electron density. Three ligands can possibly be dissociated in carboxylates **1a**−**c**. The bridging phenolate is not likely to be decoordinated because this process (i) would be hampered by the bridging carboxylates and (ii) would probably result in the destruction of the complexes what is not consistent with the observed overall chemical reversibility. Therefore we are left with possible release of either the terminal phenolate or a carboxylate group. Dissociation of the terminal phenolate is unlikely for several reasons: (i) replacing a phenolate by a pyridine as in HLPy4 induces a positive shift of the reduction potential of ca. 500 mV which is not consistent with the observed 180 mV change; (ii) in the complex of the nitro-substituted ligand $H_2L'1$ both redox couples undergo the electron withdrawing effect of the nitro group what suggests that the phenolate is coordinated in all species. Thus a carboxylate group is the ligand most likely to dissociate. This is quite in line with its well documented lability;[42] however, it is not known whether it dissociates completely or stays bound to the iron in the N_3O_3 site. As mentioned in the structural section the two carboxylates are bound asymmetrically, and in the N_2O_4 site the carboxylate bound *trans* to the phenolate is bound less strongly than the other one. This effect is likely to operate also in the diferrous derivative, and it may pave the way to dissociation of the carboxylate. At this stage it must be explained why the diphenylphosphate complex of H_2L1 and the benzoate complex of H_2L2 do not exhibit the same redox behavior. In the case of the phosphate two effects can be invoked: (i) it is less electron donating than the carboxylates as shown by the present electrochemical study; (ii) it is far less labile than carboxylates. For the carboxylate derivatives of H_2L2 (and the complexes of ligands bearing two terminal phenolates) we believe that their different behavior may originate from a structural difference

(39) Wang, D. L.; Holz, R. C.; David, S. S.; Que, L.; Stankovich, M. T. *Biochemistry* **1991**, *30*, 8187.

(40) Silva, K. E.; Elgren, T. E.; Que, L., Jr.; Stankovich, M. T. *Biochemistry* **1995**, *34*, 14093.

(41) (a) Liu, K. E; Lippard, S. J. *J. Biol. Chem.* **1991**, *266*, 12836. (b) Paulsen, K. E.; Liu, Y.; Fox, B. G.; Lipscomb, J. D.; Münck, E.; Stankovich, M. T. *Biochemistry* **1994**, *33*, 713.

(42) Drüecke, S.; Wieghardt, K.; Nuber, K.; Weiss, J.; Fleishhauer, H.-P.; Gehring, S.; Haase, W. *J. Am. Chem. Soc.* **1989**, *111*, 8622.

with **1a**−**c**. Actually, in **1a**, owing to the five-membered chelate ring including the aminophenol group, the terminal phenolic oxygen is *cis* to the bridging phenolate and *trans* to a carboxylate which it destabilizes. In the three structurally characterized diferric derivatives of the ligands with two terminal phenolates[19−21] these groups are engaged in a six-membered chelate ring and occupy positions *trans* to the bridging phenolate. As a consequence they do not exert any destabilizing influence on a carboxylate. It is likely that the same structural situation holds for the complexes of H_2L2 also.

In summary, the proposed dissociation of the carboxylate in **1a**−**c** would result both from increased electronic density provided by the terminal phenolate and concomitant destabilization of the carboxylate bound in the *trans* position.

Biological Relevance of These Model Complexes. The present compounds are the first asymmetrical diiron complexes which incorporate some of the characteristic structural features of the active sites of the PAP enzymes, namely a μ-(OR)-μ-carboxylato bridging pattern and, most importantly, the presence of a terminal phenolate ligand on a single iron atom of the pair. This similarity with the natural sites is not only structural but extends to the electronic properties, as evidenced by the congruency of several physical parameters. The Mössbauer parameters and the exchange coupling constant of the model complexes are in the range observed for the uteroferrin phosphate complex.[1,2] This is of interest because the present mixed-valent compounds do not show an EPR spectrum.[43] This is indeed a puzzling feature because antiferromagnetically coupled $Fe^{II}Fe^{III}$ systems generally exhibit EPR spectra with g values lower than 2,[44] and such spectra have been observed for related symmetrical complexes.[13−15] Nevertheless, this behavior is reminiscent of early reports that the phosphate complex of reduced Uf (Uf-r) was EPR silent. However more recent EPR and magnetization studies[45] have shown that a very broad EPR spectrum of the phosphate Uf-r complex can be detected in somehow drastic conditions. The broadness of the spectrum is due to combination of a strong g anisotropy and increased line width resulting from the fact that the exchange interaction J between the Fe^{II} and the Fe^{III} ions is comparable in magnitude to the zero-field splitting D of the Fe^{II} ion. The $|J/D|$ ratio is even smaller in **1a** ($|J/D| = 4/13$) than in the phosphate Uf-r complex ($|J/D| = 3/8$) which explains why its EPR spectrum cannot be detected even in the drastic conditions used for the protein.[43] The phenolate → Fe^{III} charge transfer band is shifted to lower energy in complexes of H_2L2 with respect to the derivatives of reduced Uf. This reflects the difference in the overall coordination sphere of the iron atoms which comprises a majority of oxygen donors in the protein as opposed to a majority of nitrogen donors in the model complexes.

The electrochemical studies have revealed a number of interesting features. One of them is the peculiar behavior exhibited by the carboxylate complexes of ligand H_2L1 in the $Fe^{II}Fe^{II}$ state where the coordination of a carboxylate is so weakened that it dissociates. This behavior is reminiscent of the release of the iron ions by dithionite treatment of the PAP enzymes. The latter process is basically the dissociation of the ligands provided by the protein backbone, and thus there is some similarity with the behavior observed here. The present study therefore provides some clues to the origin of this peculiar behavior of the PAP proteins.

Another point of interest is the role of the tyrosinate ligand and its relation to the enzyme function. The PAP enzymes in their $Fe^{II}Fe^{III}$ state are active *in vitro* for the hydrolysis of phosphates, a nonredox process. However, they are inactivated by phosphate binding which promotes oxidation to the diferric state. So it may be envisaged that the redox process be involved in the regulation of the enzyme activity. Alternatively, owing to their similarity with the other diiron proteins, the diiron PAP enzymes could be involved in some sort of dioxygen activation.[46] In this respect it is worth noting that they have been shown to react with hydrogen peroxide[47] and induce lipid peroxidation.[48] Other possibilities have been considered, such as the storage and transport of iron.[1] The electrochemical study of the present model compounds has shown that a terminal phenolate exerts a significant influence on the redox potentials of the $Fe^{II}Fe^{III}/Fe^{III}Fe^{III}$ couple. However, comparison of the redox potentials in Uf, RNR, and MMOH indicates that this influence is counterbalanced by differences in the active site surrounding. Apart from its effect on the redox potentials the tyrosinate causes a stabilization of the mixed-valent form and a destabilization of the reduced state. The former is clearly favorable to one-electron *vs* two-electron processes which might be crucial to dioxygen activation and related processes. The latter, on the other hand, could play a role in redox controled iron delivery. The function of the PAP enzymes is still a matter of debate. In this respect, the present study emphasizes some basic chemical features of the properties of these diiron systems. Clearly more work must be carried out before the activity of these enzymes can be understood at the molecular level.

Supporting Information Available: NMR data of intermediates in the ligands syntheses, elemental analysis of diiron complexes, and tables of atomic coordinates and thermal parameters for **1a** and summary of NMR data for **1a** and **2d** (6 pages). See any current masthead page for ordering and Internet access instructions.

JA970345Q

(43) We have failed to detect an EPR spectrum for **1a** in acetonitrile and acetone solutions as well as in the solid state either as a powder, a microcrystalline sample, or a single crystal even in drastic conditions (temperature: 4 K, power: 200 mW, modulation: 20 G).

(44) Bertrand, P.; Guigliarelli, B.; More, C. *New J. Chem.* **1991**, *15*, 445.

(45) Day, E. P.; David, S. S.; Peterson, J.; Dunham, W. R.; Bonvoisin, J.; Sands, R. H.; Que, L. *J. Biol. Chem.* **1988**, *263*, 15561.

(46) Dietrich, M.; Münstermann, D.; Suerbaum, H.; Witzel, H. *Eur. J. Biochem.* **1991**, *199*, 105.

(47) Hayson, A. R.; Cox, T. M. *J. Biol. Chem.* **1994**, *269*, 1294.

(48) Vallet, J. L. *Biol. Reprod.* **1995**, *53*, 1436−1445.